İSTANBUL TECHNICAL UNIVERSITY ★ INSTITUTE OF SCIENCE AND TECHNOLOGY

MACHINIBILITY OF ZIRKONIUM BASED BULK METALLIC GLASS ON DRILLING & MILLING

M.Sc. Thesis by

Veli NAKŞİLER, B.Sc.

Department : Mechanical Engineering

Programme : Material and Manufacturing

Supervisor : Assist. Prof. Dr. Mustafa BAKKAL

JUNE 2008

İSTANBUL TECHNICAL UNIVERSITY ★ INSTITUTE OF SCIENCE AND TECHNOLOGY

MACHINIBILITY OF ZIRKONIUM BASED BULK METALLIC GLASS ON DRILLING & MILLING

M.Sc. Thesis by
Veli NAKŞİLER, B.Sc.
(503051315)

Date of submission : 5 May 2008

Date of defence examination: 9 June 2008

Supervisor (Chairman): **Assist. Prof. Dr. Mustafa BAKKAL**

Members of the Examining Committee **Assoc. Prof. Dr. İsmail LAZOĞLU**

Assist. Prof. Dr. Muzaffer ERTEN

JUNE 2008

İSTANBUL TEKNİK ÜNİVERSİTESİ ★ FEN BİLİMLERİ ENSTİTÜSÜ

ZİRKONYUM ESASLI KALIN CAMSI METALLERİN FREZE VE DELİK DELMEDEKİ İŞLENEBİLİRLİĞİ

YÜKSEK LİSANS TEZİ
Müh. Veli NAKŞİLER
(503051315)

Tezin Enstitüye Verildiği Tarih : 5 Mayıs 2008
Tezin Savunulduğu Tarih : 9 Haziran 2008

Tez Danışmanı : Yrd. Doç. Dr. Mustafa BAKKAL
Diğer Jüri Üyeleri Doç. Dr. İsmail LAZOĞLU
Yrd. Doç. Dr. Muzaffer ERTEN

HAZİRAN 2008

ACKNOWLEDGEMENTS

I would like to first thank my advisor, Asst. Prof. Mustafa Bakkal. This dissertation could not have been written without him who not only served as my supervisor but also encouraged and challenged me throughout my academic program. He directed me to a wide range of resources on the web and in the library stacks. He answered all of my questions as well as asked me questions that helped me to narrow my search. I am grateful in every possible way and hope to keep up our collaboration in the future.

I gratefully acknowledge Asst. Prof. İsmail Lazoğlu, head of the Manufacturing Automation and Research Center at Koc University, for his advice, and crucial contribution, which made him a backbone of this research and so to this thesis.

Many thanks go in particular to Sami Fidanlı, Osman Çelebi and Erdal Dinç who are the skillful technicians of ITU Mechanical Engineering Faculty, assisted me during the setting up my experimental equipments.

Finally, I want to very special thanks to my family for their consistent support and belief in me.

December 2007 Veli NAKŞİLER

TABLE OF CONTENTS

ABBREVIATION

BMG	: Bulk Metallic Glass
WC	: Tungsten Carbide
MG	: Micrograin
DAQ	: Data Acquisition Card
PC	: Personal Computer
SEM	: Scaning Electron Microscope
KEP	: Kinetic Energy Penetrator
HSS	: High Speed Steel
GFA	: Glass Forming Ability

LIST OF TABLES

LIST OF FIGURES

MACHINIBILITY OF ZIRCONIUM BASED BULK METALLIC GLASS ON DRILLING AND MILLING

SUMMARY

Metallic glasses were discovered over forty years ago when rapid quenching methods were first applied to Au-Si system. During the past several years, advances have been made in this field as a result of the discovery and development of several families of alloys with substantially improved glass forming ability. Whereas previous metallic glasses were generally formed by cooling the melt at rates of 10^5–10^6 K s^{-1}, the more recently developed alloys require cooling rates of only 1–100 Ks^{-1} or less. As such, the new materials can be cast from the molten state into glassy objects with dimensions up to several centimeters as compared with maximum thickness or diameter of 10–100 μm for rapidly quenched ribbons and powders. These new alloys are referred to as 'bulk glass formers' or 'bulk metallic glasses'.

Bulk metallic glasses are amorphous alloys with no long-range periodic lattice structure, which exhibit unique mechanical, thermal, and magnetic properties. Metallic glasses are also called as amorph alloys and non-crystalline alloys. Most metals do crystallize as they cool. But if crystallization does not occur, and the atoms settle into a nearly random arrangement, the final form is a metallic glass. There are no grain boundary and dislocation in their structure therefore they exhibit superior properties when compared with similar crystalline structure metals. In recent years, production of new metallic glasses in bulk form is getting popular because of their superior strength, elasticity and magnetic properties. Thanks to new alloy systems, the production of bulk metallic glasses with thicker section has been achieved in recent years. Developments in BMG, designate it as a promising material in near future especially for strategic and structural applications. Beside their superior mechanical, elastic and magnetic properties, BMGs have characteristic wear and corrosion properties. These properties are high strength, high hardness, high strength/density ratio, no strain hardening, high wear and corrosion resistance and high elasticity.

In this study, to investigate the machinability of Zr-based BMG ($Zr_{52.5}T_{i5}Cu_{17.9}Ni_{14.6}Al_{10}$), a set of drilling and milling experiments were conducted. During all experiments, piezoelectric dynomemeter and thermal camera were used to measure excited cutting forces and maximum temperatures, respectively. BMG having with a 6.5 mm diameter was casted by arc melting method and machined after cut to 2 mm thickness disks. No chip light emission was observed during all the tests.

Drilling experiments were conducted at constant spindle speed and at different feed rates by using different tool materials. Spindle speed was 2500 rpm and tool materials were TiAlNi coated Solid-WC, uncoated MG-WC and HSS. The chip and burr morphology were examined by SEM. Two types of chip morphology (ribbon shape snarled and helical shape snarled) and crown shaped exit burr formation are observed in drilling of BMG. Best results on exit burr formation, minumum temperature and hole surface roughness is obtained while using MG-WC tool on BMG drilling.

Milling experiments were conducted at constant axial depth of cut and spindle speed. Spindle speed and axial depth of cut were 5000 rpm and 0.5 mm, respectively. Two different tool paths, spiral and slot milling, were used. Slot milling was selected to simplfy the cutting mechanics analysis. Spiral milling was preferred to use the limited BMG efficiently by creating the longest possible tool path. Two different tool materials, WC and HSS, cut the work material during the experiments. The chip and burr morphology were examined by SEM and optic microscope. Cutting mechanics of helical end mill was investigated for a specified cutting speed range and the cutting coefficients for BMG-WC workpiece-tool pair were identified by using mechanistic approach. Cutting forces of slot milling were modeled analytically by using cutting coefficients and were compared with the experimentally measured forces. The results converge to the real values with less than %5 error.

ZİRKONYUM ESASLI CAMSI METALLERİN FREZE VE DELİK DELMEDEKİ İŞLENEBİLİRLİĞİ

ÖZET

Camsı metaller ilk kez günümüzden kırk yıl önce Au-Si alaşımının hızlı soğutulması sonucu üretilmiştir. Son yıllarda ki gelişmeler sayesinde iyileşen camlaşma yetisi ilk zamanlarda 10^5-10^6 °C\s olan soğuma hızını 0.1-100 °C\s hızlarına indirmiştir. Bu gelişmelerin neticesinde kesit kalınlığı 10–100 μm arasında değişen şerit şeklindeki camsı metalden kalınlığı birkaç cm'yi bulan "kalın camsı metaller" üretilmiştir.

Kalın camsı metaller, amorf yapıya sahip ve hızlı katılaşma sonucunda atomların sıvı hal pozisyonlarının katı halde de korunduğu ve bu yapısal özelliği sayesinde de üstün mekanik, ısıl ve manyetik özellikler gösteren malzemelerdir. Camsı metaller ayrıca, amorf alaşımlar veya kristal olmayan alaşımlar diye de adlandırılmaktadır. Soğurken kristalleşen birçok metalin aksine camsı metallerde atomlar arasında düzenli bir yapı mevcut değildir. Mikro yapılarında tane sınırı ve dislokasyon bulunmaz, bu yüzden de benzeri kristal yapılı malzemelere göre birçok açıdan üstün özellikler sunmaktadır. Üstün dayanım, elastisite ve manyetik özellikleri sayesinde kalın kesitte camsı metal üretimi üzerine olan rağbet son yıllarda oldukça artmıştır. Yapılan araştırmaların sonucunda camsı metallerin üretimlerini kısıtlayan hızlı soğutma zorunluluğunun, bulunan yeni alaşım sistemleriyle aşılmasıyla daha kalın kesitlerde de üretimi başarılmıştır. Bu gelişmeler, camsı metallerin özellikle stratejik uygulamalar başta olmak üzere yapı malzemesi olarak ta yakın gelecekte yaygın olarak kullanılacağını işaret etmektedir.

Camsı metaller üstün mekanik, elastik ve manyetik özelliklerinin yanında, kendine özgü aşınma ve korozyon davranışlarına da sahiptir. Bu özellikler; yüksek dayanım, yüksek sertlik, yüksek dayanım/yoğunluk oranı, pekleşmeme, %2'ye kadar çıkabilen elastiklik sınırı, yüksek korozyon dayanımı, yüksek aşınma dayanımı, döküm sonrası düşük veya hiç görülmeyen kendini çekme şeklinde sayılabilir.

Bu çalışmada, Zirkonyum esaslı KCM ($Zr_{52.5}T_{i5}Cu_{17.9}Ni_{14.6}Al_{10}$), talaşlı imalat yöntemlerinden delik delme ve frezeleme işlemlerine tabi tutuldu ve işlenebilirliği incelendi. Her iki işleme sırasında oluşan kesme kuvvetleri piezoelektrik dinamometreyle, ulaşılan maksimum kesme sıcaklığıda termal kamerayla ölçüldü ve

hiçbir delme ya da frezeleme işlemi sırasında kristalleşme ya da yanma gerçekleşmedi. Bütün deneylerde arkla ergitme yöntemiyle üretilen 6.5 mm çapında KCM, 2 mm kalınlığında diskler halinde kesilerek işlendi.

Delik delme işlemleri sabit devirde, farklı ilerleme hızları ve takım malzemeleri kullanılarak yapıldı. Delik delme işlemlerinde TiAlNi kaplı Solid-WC, kaplamasız MG-WC ve HSS takımlar kullanıldı. Bütün deneyler 2500 devir hızında gerçekleştirildi ve kesme sonucu oluşan talaşın ve çapağın morfolojisi SEM kullanılarak incelendi. Yapılan testlerde şerit ve helis şeklinde takımı saran iki tip talaş formu ve taç yapısında çapak oluşumu gözlendi. Her bir deliğin yüzey pürüzlülüğü ölçüldüğünde MG-WC takımla delinen malzemede daha iyi sonuçlar alındı. En yüksek ilerleme kuvveti yaklaşık %15 farkla MG-WC takımda, en yüksek sıcaklıksa Solid-WC takımla delinen malzemede görüldü.

Frezeleme deneyleri de sabit devir, sabit kesme derinliği, farklı ilerleme hızları ve iki farklı takım yolu kullanılarak yapıldı. Bu takım yollarından kanal frezleme, kesme mekaniği analizleri, spiral frezeleme de, takım malzemeden ayrılmadan en uzun kesme yapılabilmesi ve eldeki sınırlı KCM'i en verimli şekilde değerlendirmek için oluşturuldu. Spiral takım yolu kullanılarak yapılan kesimler sonucu elde edilen talaşlar mikroskopla incelendiğinde şerit ve iğnemsi biçimde iki tip standart talaş formu gözlendi. Bu talaşlardan daha ideal olan iğnemsi form 0.5 ve 1 µm\diş ilerlemeyle yapılan kesimlerde görüldü. Kesme deneyleri HSS ve WC takımlar kullanılarak gerçekleştirildi. Kanal frezeleme sonucu oluşan çapağın morfolojisi SEM ve optik mikroskopla incelendi ve sabit kesme hızında ilerleme hızı arttıkça kanalın bir kenarında biriken çapak miktarında ve yüzey pürüzlülüğünde de artış olduğu saptandı. Ayrıca frezenin kesme mekaniği incelendi ve kalın camsı metal (KCM) ve WC helisel freze takımı (takım malzeme çifti) için belli bir kesme hızı aralığında mekanistik yöntem kullanılarak kesme sabitleri hesaplandı. Bu kesme sabitleri kullanılarak kanal frezelemede oluşan kuvvetler analitik olarak modellendi ve deneysel olarak ölçülen kuvvet değerleriyle karşılaştırıldığında %5'in altında bir hata oranıyla gerçek değerlere yaklaşıldığı görüldü.

1. INTRODUCTION

BMGs are amorphous metals with critical cooling rates low enough to allow formation of amorphous structure in thick layers (over 1 millimeter). An amorphous metal is a metallic material with a disordered atomic-scale structure and it has no grain boundary. Therefore, BMGs are also called as glassy alloys, amorphous alloys or non-crystalline alloys.

Since it is relatively new group of material, most of the academic researches focused on micromechanics of bulk metallic glass of materials [1-2]. Limited work done so far about machining of BMG [3-4]. Early drilling study for 1 mm drill, shows that HSS tools and high spindle speed creates light emission and oxidation during drilling. Choosing the correct tool material and process parameters have crucial importance for creates good surface finish and successful machining process [3].

Due to the unique properties of this new material such as mechanical, thermal, magnetic and corrosive, various applications can be applied [1].

In this research drilling and milling of casted Zr-based BMG ($Zr_{52.5}T_{i5}Cu_{17.9}Ni_{14.6}Al_{10}$) shown in Figure 2.1 were studied. In drilling, the effects of feed rate and tool material on the chip, burr formation and thrust force with the varying feed rate at the constant spindle speed (2500 rpm) were investigated. To investigate the behavior of BMG in drilling by two different tools at different feed rates, two sets of drilling experiments are first introduced in this paper.

Figure 2.1: Zr-based BMG Button and Ingot Prepared by Arc Melting and Drop Casting in Inert Gas Atmosphere

Figure 2.1 shows the Zr-based BMG button and ingot prepared by arc melting and drop casting in inert gas atmosphere in Oak Ridge National Laboratory (ORNL).

In milling, cutting mechanics of helical end mill was examined. The cutting coefficients for BMG-WC workpiece-tool pair were identified by using mechanistic approach. Analytically modeled forces converge to the experimentally measured forces with less than 5% error. Analyzing of chip and burr formation of slot and spiral milling operations showed that the rollover and top burr formation were observed in slot milling and needle like and ribbon type chips were observed in spiral milling operations.

In conclusion, machining performance of $Zr_{52.5}Ti_5Cu_{17.9}Ni_{14.6}Al_{10}$ metallic glass under different milling and drilling parameters was evaluated. Evaluation was not carried out only in the mechanics of machining but also characterization of BMG chips in the microstructural point of view. Chip light emission, chip morphology, cutting mechanics, burr formation of Zr-based BMG due to milling and drilling of Zr-based BMG are studied throughout the research. According to analyzing of chip morphology and burr formation of drilling holes and milling slots optimum range of process parameters are investigated to increase the machining quality.

2. BULK METALLIC GLASS

2.1 Historical Backround of BMG

Glass is any material that can be produced by preventing the crystallization during the solidification. Most metals do crystallize as they cool, arranging their atoms into a highly regular spatial pattern called a lattice. But if crystallization is prevented by fast cooling, and the atoms settle into a nearly random arrangement, the final form is a metallic glass. In recent years, production of new metallic glasses mostly by nearly conventional casting techniques in bulk form is getting popular because of their superior strength, elasticity, magnetic properties and corrosion resistance [5]. Metallic glasses are called as bulk metallic glass when the sample thickness is bigger than 1 mm. Today producing bulk metallic glasss with the sample thickness of ~ 80 mm is possible [18].

The first metallic glass was discovered in 1960 when rapid quenching methods were first applied to Au-Si system by Duwez at al. This discovery is carried out the first worked on the technique known as "splat cooling" shown in Figure 3.2 which achieves cooling rates in the range 10^6-10^8 $^\circ$C/s as liquid alloy is solidified. In this technique, liquid droplets of the alloy are shot from a carbon dioxide gun onto a cooled Cu or Ag block to produce solid "splats". This amorphous structure was metastable and could be converted into a metastable crystalline phase by annealing [6, 7].

Suppressing the crystallization, one of the crucial steps to get low critical cooling rate for bulk metallic glasses has enabled with the discovery of new compositions. The glass forming ability (GFA), combination of large differences in atomic size of the constituent elements and negative heat of mixing hinder local atomic rearrangements in the undercooled liquid state are other important thermodynamic and kinetic criteria to get bulk metallic glasses.

During the past several years, advances have been made in this field as a result of the discovery and development of several families of alloys with substantially improved glass forming ability. Whereas previous metallic glasses were generally formed by cooling the melt at rates of 10^5–10^6 K s^{-1}, the more recently developed alloys require cooling rates of only 1–100 Ks^{-1} or less. As such, the new materials can be cast from the molten state into glassy objects with dimensions up to several centimeters as

compared with maximum thickness or diameter of 10–100 μm for rapidly quenched ribbons and powders. These new alloys are referred to as 'bulk glass formers' or 'bulk metallic glasses'.

The work of the David Turnbull and his group in the early 1960s was another critical contribution to the subject [8]. This work illustrated the similarities between metallic glasses, ceramic glasses and silicates. Specifically, Turnbull, Chen, and other later collaborators clearly demonstrated the existence of a glass transition in rapidly quenched Au-Si glasses as well as the other Pd-Si and Pd-Cu-Si glass forming alloys synthesized initially by the Duwez group [9].

The field of metallic glasses gained momentum in the early 1970's when Allied Chemical Corporation developed continuous casting processes for commercial manufacturing of metallic glass ribbon and sheets [10]. During the same period, Chen and collaborators used simple suction casting method to form millimeter diameter rods of ternary Pd-Cu-Si alloys at significantly low cooling rates in the range of 10^3 K/s [11]. The synthesis of metallic glasses in a bulk form (with thickness >1 mm) was successfully achieved in $Ni_{40}Pd_{40}P_{20}$ alloys in 1976 [12].

During the late 1980s, Akihisa Inoue and his coworkers in Sendai, Japan, found exceptional glass forming ability in the rare-earth rich alloys [13], e.g. La-Al-Ni and La-AL-Cu. By casting the alloys into copper molds, they fabricated fully glassy rods and bars with cast thickness of several mm. From there, they studied similar quaternary and quinary materials (e.g. La-Al-Cu-Ni) and developed alloys that formed glass at cooling rates under 100 K/s with critical casting thickness ranging upward toward 1 cm [14].

A similar family of alloys, with the rare-earth metal partially replaced by the alkali earth metal Mg were also developed along with the parallel family of multi component Zr-base alloy (e.g. Zr- Cu-Ni-Al) [15]. The work opened the door to develop of the other broad classes of bulk metallic glasses. Building on the Inoue work, Peker and Johnson [16] developed a family of ternary, quinary and higher order glass formers based on higher order alloys of Zr, Ti, Cu, Ni, Be (also combined with other transition metals, TM). One extensively studied example, referred to as Vitreloy 1, has a composition of $(Zr_3Ti)_{0.55}(Cu_5Ni_4)_{0.225}\,Be_{0.225}$. Critical cooling rate for glass formation are 1 K/s. The alloys were cast in the form of fully glassy rod with diameters ranging up to 5–10 cm. The alloys require no fluxing or special processing treatments and form bulk glass by conventional metallurgical casting methods [9].

Since 1988, bulk glass formation has been reported in various alloys based on Cu, Ti, Fe, Nd, and Pr. But these alloys generally have small supercooled regions and their

critical sizes for glass formation are generally smaller than that (30 mm) of Zr based alloys. However, with attention back to Pd based alloys recently, large glass formation by water quenching using B_2O_3 flux has been reported in $Pd_{40}Cu_{30}Ni_{10}P_{20}$ alloy with diameter up to 72 mm [17], which is the largest size of bulk metallic glasses reported so far [18].

Table 2.1 summarizes production methods section thicknesses for glass formation in chronological order and bulk glass formation in different alloy systems respectively.

Table 2.1: Production Methods and Section Thicknesses of Bulk Glass Forming Alloys in Chronological Order

Year	Alloy	Thickness (mm)	Method
1969	Pd-Cu-Si	1	Splat quenching
1978	$Pd_{72}Cu_6Si_{16}$	0.9	Water quenching
1981	$Pd_{78}Cu_6Si_{16}$	1.50	Low gravity tube dropping
1981	$Pd_{77}Cu_6Si_{17}$	0.75	Bridgman solidification
1982	$Au_{55}Pb_{22.5}Sb_{22.5}$	1,50	Liquid quenching
1984	$Pd_{40}Ni_{40}P_{20}$	10	Water Quenching Casting with B_2O_3 flux
1990	$La_{55}AL_{25}Ni_{20}$	3	Metallic mold casting
1991	$Mg_{65}Cu_{25}Y_{10}$	4	Metallic mold casting
	$Zr_{57}Ti_5Al_{10}C_{20}Ni_8$	20	Mold casting
	$Zr_{65}Al_{7.5}Ni_{10}Cu_{17.5}$	7	Chill casting
1992	$Mg_{65}Cu_{25}Y_{10}$	7	High pressure die casting
1993	$Zr_{65}Al_{7.5}Ni_{10}Cu_{17.5}$	16	Water quenching
	$La_{55}Al_{25}Ni_{10}Cu_{10}Co_5$	> 9	High pressure die casting
	$Zr_{41.2}Ti1_{3.8}Ni_{10}Cu_{12.5}Be_{22.5}$	14	Water quenching
1994	$Nd_{60}Al_{15}Co_{10}Cu_{10}Fe_5$	> 6	Injection mold casting
1995	$Fe_{73}Al_5Ga_2P_{11}C_5B_5$	1	Injection casting
1996	$Pd_{40}Ni_{10}Cu_{30}P_{20}$	40	Water quenching
	$Zr_{55}Al_{10}Ni_5Cu_{30}$	30	Suction casting
	$Pd_{40}Ni_{40}P_{20}$	25	Water quenching
	$Nd_{60}Fe_{30}Al_{10}$	15	Suction casting
1997	$Pd_{40}Ni_{10}Cu_{30}P_{20}$	72	Water quenching
2002	$Fe_{67}Co_{9.5}Nd_3Dy_{0.5}B_{20}$	0.5	Powder consolidation
2003	$(Fe_{0.75}B_{0.15}Si_{0.1})_{96}Nb_4$		Injection casting
	$Fe_{75}Ga_3P_{9.5}C_4B_4\ Si_{2.5}$	2	
2004	$Co_{43}Fe_{20}Ta_{5.5}B_{31.5}$	Ring	Copper mold casting
	$Fe_{75.5}Ga_3P_{10.5}C_4B_4\ Si_3$		
	$Cu_{46}Zr_{44}Al_7Y_5$	10	Copper mold casting
2005	$Cu_{50}Zr_{50}$	1	

Table 2.1: Production Methods and Section Thicknesses of Bulk Glass Forming Alloys in Chronological Order (cont.)

	Zr-Cu-Al	8	
2006	$Cu_{45}Zr_{45}Ag1_0$	6	Copper mold casting
	$(Cu_{0.6}Hf_{0.25}Ti_{0.15})_{90}Nb_{10}$	2	
	$Cu_{40}Zr_{44}Ag_8Al_8$	15	
2007	$La_{65}Al_{14}(Cu_{5/6}Ag_{1/6})11(Ni_{1/2}Co_{1/2})_{10}$	30	Water quenching
	$Fe_{63}Ni_7Zr_6Cr_8W_3Si_3B_{10}$		Twin roll strip casting
	$Fe_{74}Ni_9Cr_4Si_3B_{10}$	2	Melt spinning
	$Gd_{60}Co_{25}Al_{15}$	5	Copper mold casting
	$Gd_{60}Co_{15}Al_{25}$	4	
	$Ni_{60.25}Nb_{39.75}$	1	Copper mold injection
	$Zr_{49}Cu_{46}Al_5$	5	
	$Ti_{50}Cu_{28}Ni_{15}Sn_7$		Powder consolidation
	$Ni_{62}Nb_{33}Zr_5$	7	
	$Mg_{65}Cu_{20}Zn_5Y_9Zr_1$	2	Copper mold casting
	$Fe_{68}Mo_4Y_6B_{22}$	6.5	Copper mold injection
	$Fe_{69}Mo_3Y_6B_{22}$	6	
	$Cu_{50}Zr_{45}Ti_5$	2.5	Copper mold casting
2008	$Cu_{43}Zr_{40}Ag_7Ti_{10}$	7	Copper mold casting
	$Mm_{60}Al_{20}Co_{20}$	5	
	$Mm_{65}Al_{10}Co_{25}$	10	
	$RE_{65}Al_{20}Co_{20}$	15	
	$Fe_{68.7-x}C_7Si_{3.3}B_{5.5}P_{8.7}Cr_{2.3}Mo_{2.5}Al_2Co_x$	6	

RE: La, Ce, Pr and Nd

3. MANUFACTURING & MECHANICAL PROPERTIES OF METALLIC GLASSES

Discovery of amorphous metals begin with the rapid quenching techniques which provide very high cooling rates over 10^7 °C/s during solidification. However, these high cooling rates have limited the section thicknesses of metallic glasses into a few microns. Fortunetly, developments and innovations on metallic glass compositions and production methods during the fourty years make bulk metallic glass production possible with less than 1°C/s cooling rate. Figure 3.1 summarize the production methods of metallic glasses from beginning to today.

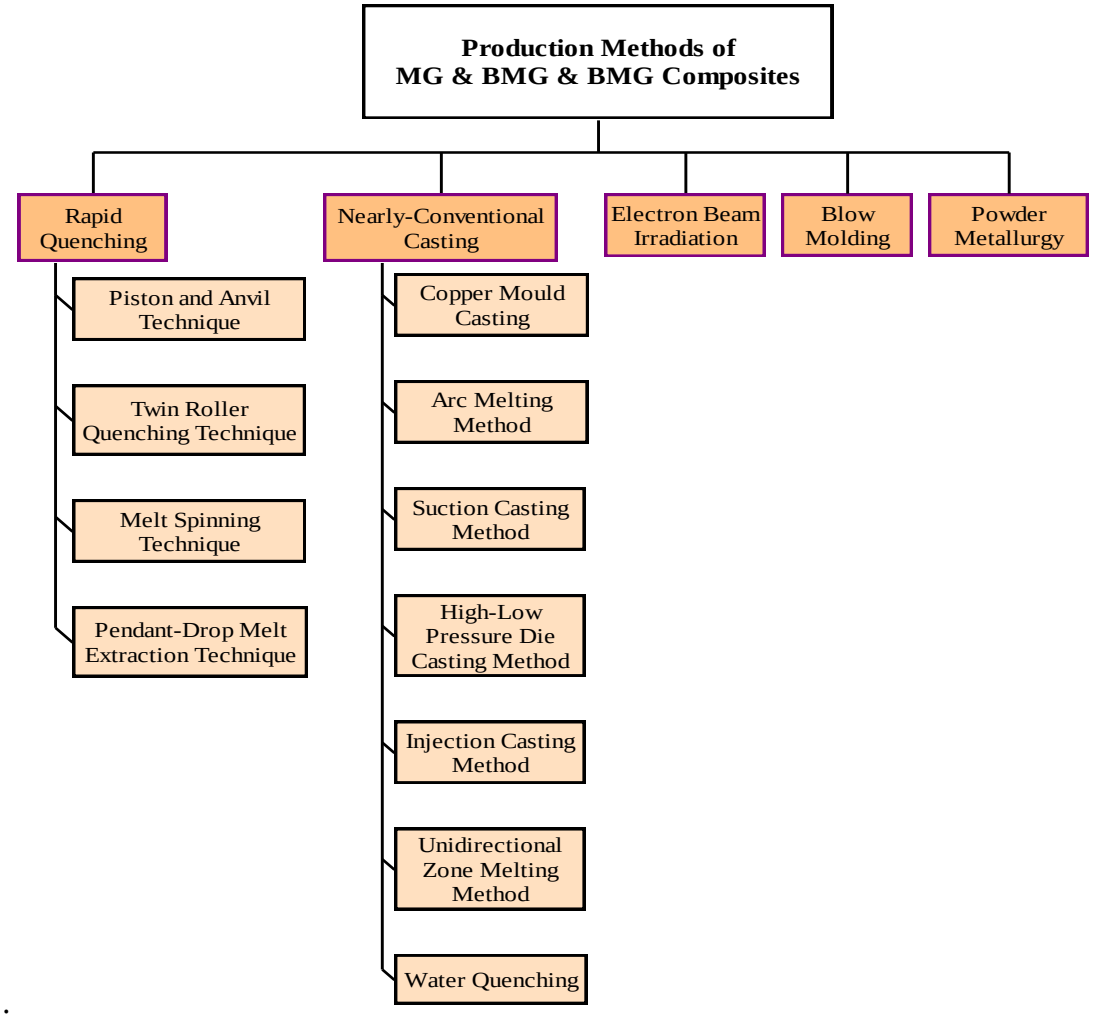

.

Figure 3.1: MG Production Methods

3.1 Rapid Quenching of MG

The first amorphous metallic alloy, $Au_{75}Si_{25,}$ was produced by Duwez et al in 1960 [6] by applying a rapid quenching method with a cooling rate of ~ 10^8 °C\s. This method was discovered by them and known as splat quenching or piston and anvil technique shown in Figure 3.1. To understand the mechanical properties of metallic glass, the first amorphous metallic alloys were not proper on account of shape and size. The following years, new rapid quenching methods like twin roller, melt spinning and pendant-drop melt extraction techniques were developed and achieved restrictions on dimensions partly. Especially, melt spinning method enabled mass production of ribbon metallic glass. All these rapid quenching techniques used in production of metallic glass were based on rapid quenching with a cooling rate range of 10^4 -10^8 °C\s. Figure 3.2 shows schematic plots of these four techniques.

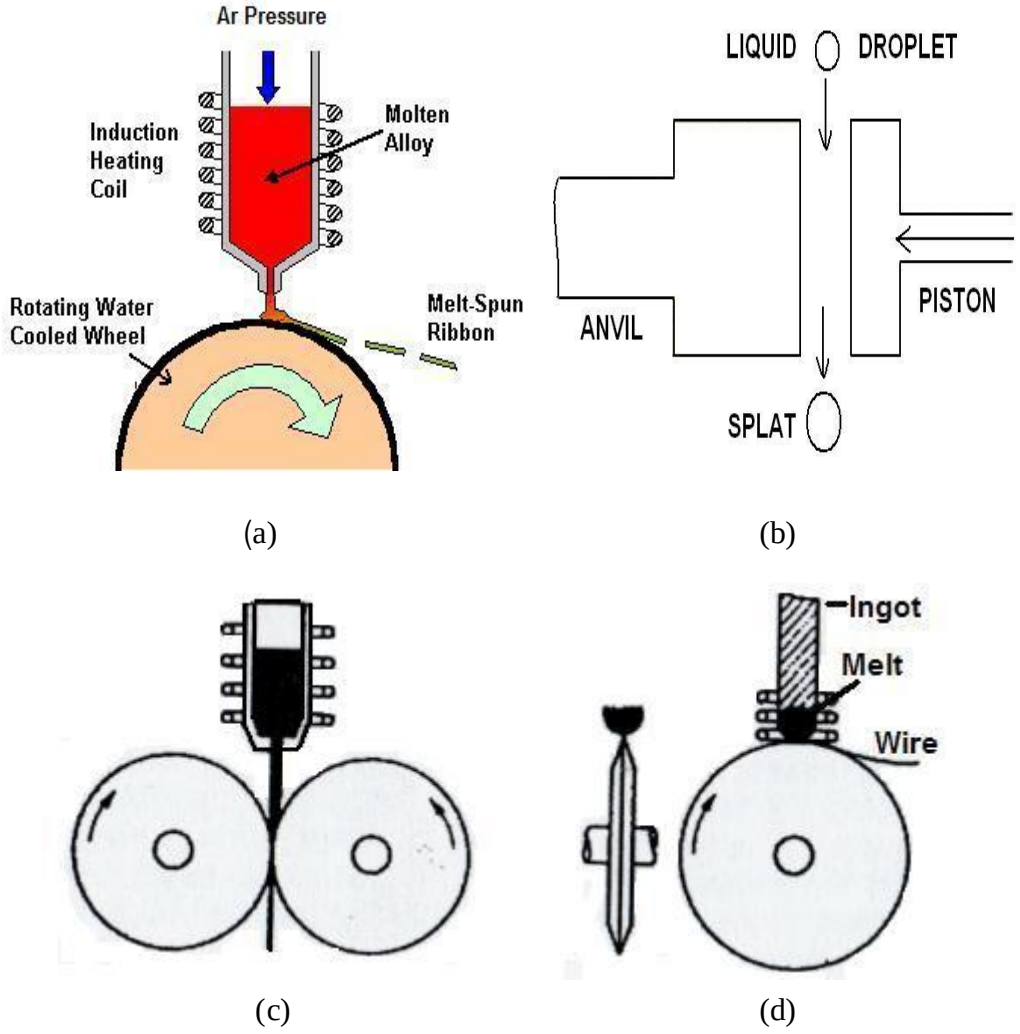

Figure 3.2: Melt-Spinning Techninique [19] (a) Splat-Cooling Technique (piston and anvil) [19] (b) Twin Roller Quenching Technique (c) Pendant Drop Melt Extraction Method (d)

3.2 Nearly-Conventional Casting of BMG

In spite of the fact that amorphous metallic glasses have promising properties, using them as structural materials were inconceivable because of their thin sections (ribbons, sheets, strips …) usually below than 1 mm. This was simply stem from relatively high cooling rates during solidification. They couldn't be produced in thick sections (above than 1 mm) till the mid of 1980s. In 1984, the maximum section thickness of 10 mm bulk metallic glass, $Pd_{40}Ni_{40}P_{20}$, was produced by Kui et al by using water quenching with a flux threatment using B_2O_3. The following years new BMGs were developed with diameters up to 80 mm by using various casting methods shown in Figure 3.1.

The BMG machined in this study was produced by arc melting on a copper hearth shown in Figure 3.3 [19]. Also, Figure 3.4 represents the low pressure die casting [26] and copper mould casting methods [27] schematically.

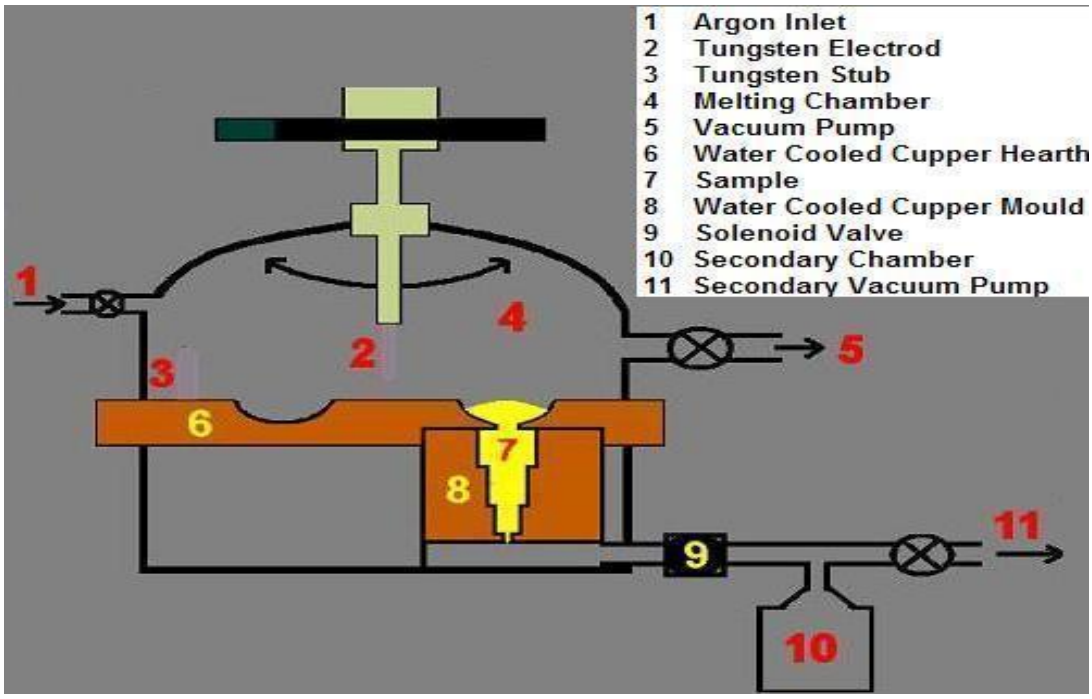

Figure 3.3: Schematic Diagram of The Arc Melting/Suction-Casting Furnace

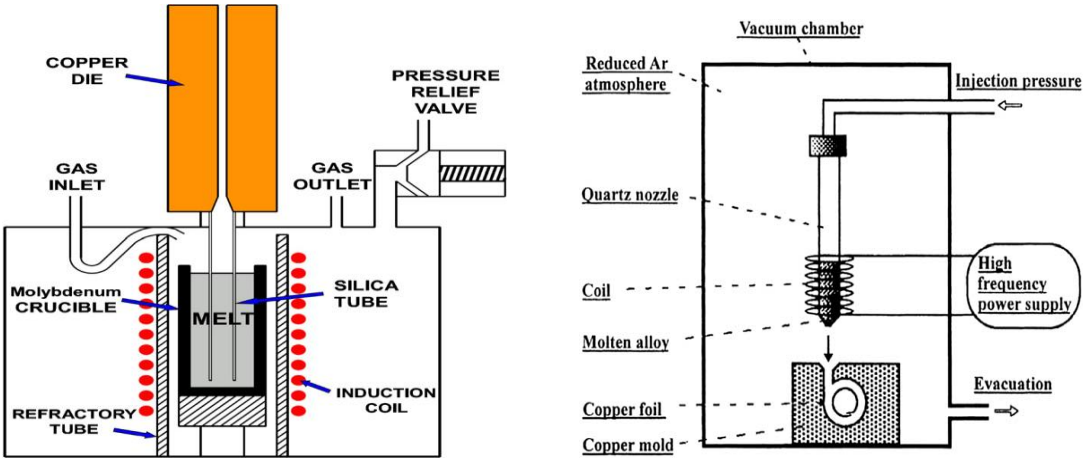

(a) (b)

Figure 3.4: A Schematic Representation of The Low-Pressure Die-Casting Unit (a) and A Copper Mold Casting Equipment (b)

3.3 Powder Metallurgy

One of the common production methods of BMGs is rapidly cooling it from the liquid state in a copper mold. Although remarkable improvements have been achieved in some high-glass forming ability material groups like Zr-based and Ti-based, there are still geometrical restrictions to solve [28]. Therefore to produce BMG apart from thin rods and sheets , powder metallurgy is a promising technology for the future of BMG [29,30]. Because metallic glasses exhibit Newtonian viscous flow in the supercooled liquid region and this allows metallic glass powders for synthesis of bulk form. In this area, Spark-plasma sintering which is a combination of hot pressing and electric current sintering, is used with mechanical alloying of BMG powders [31]. $Ti_{50}Cu_{25}Ni_{20}Sn_5$ is a sample of mechanically alloyed and spark-plasma sintered BMG fabricated by Choi et al [32] (showing nearly full density).

3.4 Blow Molding

Blow molding is a net shape process to form plastically deformable parts with complex geometries. Although BMGs has a very limited plasticity [33,34], it was realized that BMGs can exhibit appreciable plasticity in small dimensions [35]. This ability of BMGs was discovered in the beginning of the metallic glass research [38,39] and was used in various applications like synthesis of amorphous metallic alloys, net-shape processing [37,40], extrusion [43–44], superplastic forming of sheet metals [45,34], micro-and nanoreplication [36,41,42] and synthesis of BMG composites [46,47]. The first aim of the blow molding process is to eliminate the friction (physical contact) between the mold and BMG and to leave minumum stress

required for BMG forming. The process is ended when the BMG touches the surface of the mold or by realising the pressure difference. Figure 3.5 represents the schematic view of the blow molding [48].

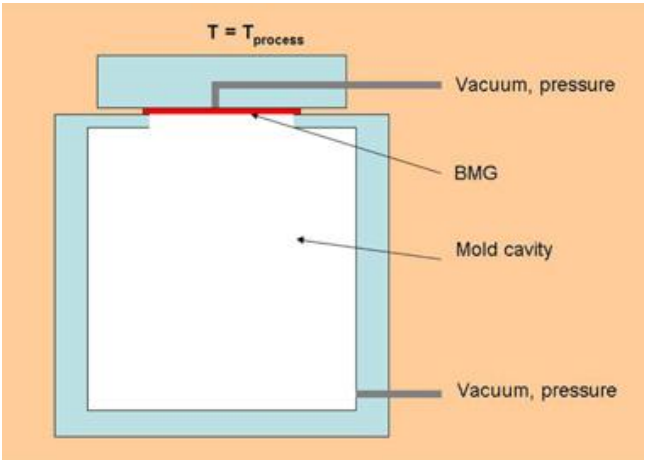

Figure 3.5: Schematic Sketch of The Blow Molding Setup

3.5 Electron Beam Irradiation

BMG alloys have excellent and unique mechanical and physical properties for structural applications. But their low ductility and elastic strain limit their usage for huge structures. Therefore humanity cannot utilize from the superior properties of these alloys completely. To overcome this issue, scientists have being developed new fabrication and forming techniques for BMG. One of these techniques is high-energy electron-beam irradiation of amorphous powders laid down on a Cu surface. By this technique surface of the material is covered with BMG alloy and interior part of the material remains same. So thanks to BMG/metal surface composite, the sufficient ductility and fracture toughness is obtained with advances of BMG alloy [49]. Figure 3.6 shows the section view of the electron beam irrediated BMG/metal surface composite.

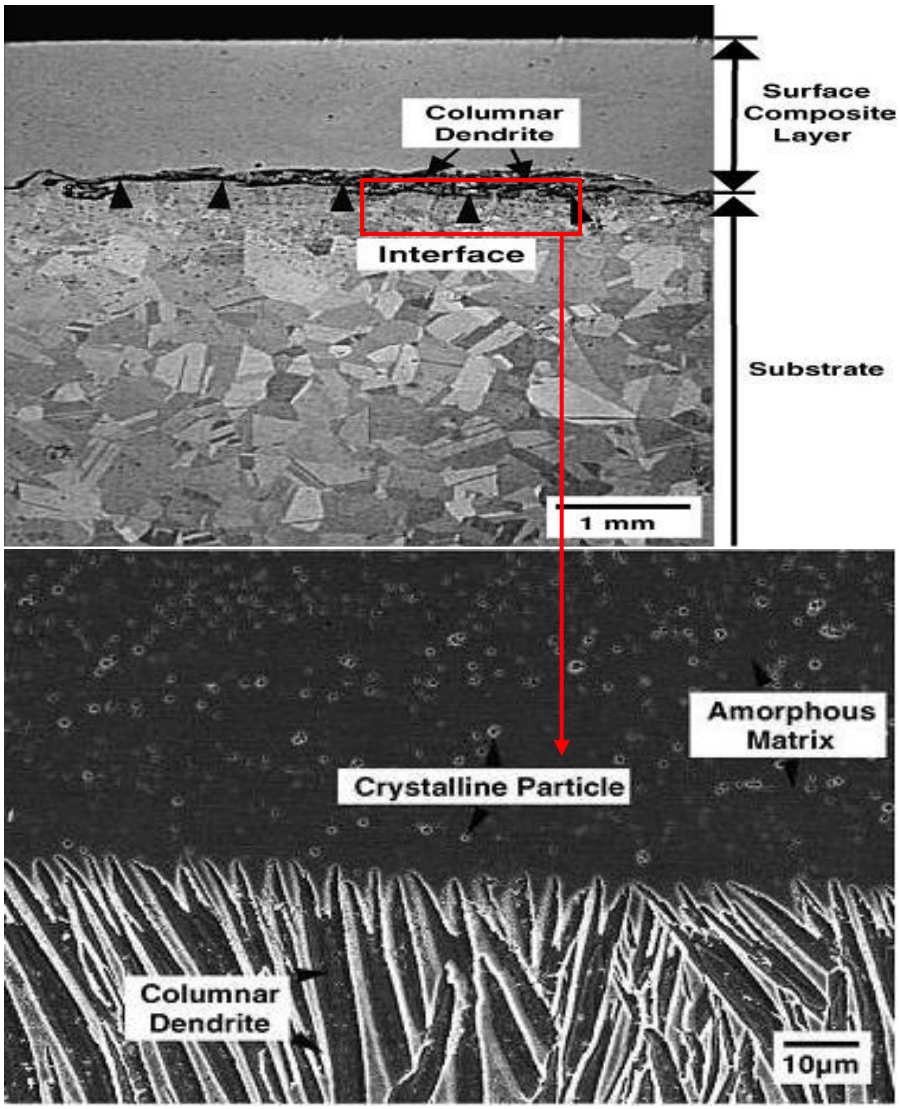

Figure 3.6: SEM and Low Magnification Views of The Electron Beam Irrediated BMG/Metal Surface Composite.

3.6 Porous BMG (Amorphous Metal Foam)

Because of high ductility in compression of amorphous metal foams, many researches were focused on to fabricate porous BMG [51]. Qiu et al [50] developed a new process, SPF (Superplastic Foaming), to fabricate BMG foam. In this method, salt and amorphous powder were mixed at specified ratios and then put in a copper can which was sealed and outgassed. After that copper can was heated isothermally and compacted into a preform. Finally the amorphous powder was deformed plastically in supercooled liquid region during the hot pressing and BMG foam was obtained successfully.

3.7 Mechanical Properties of BMG

The atomic structure is the most striking characteristic of the BMG alloy as it fundamentally differentiates BMG alloy from ordinary metals.

The atomic structure of ordinary or conventional metals and alloys is periodic, where the layout of atomic elements shows repeating patterns over an extended range. This atomic structure is called "crystalline" and limits the overall performance of conventional metals. BMG alloy possesses an "amorphous" atomic structure, which is truly unique. By contrast to the crystalline structure, no discernable patterns exist in the atomic structure of the unique BMG alloy. As such, properties superior to the limits of conventional metals can be achieved. The difference between the crystal and amorphous atomic structures can be seen in the Figure 3.7 [22].

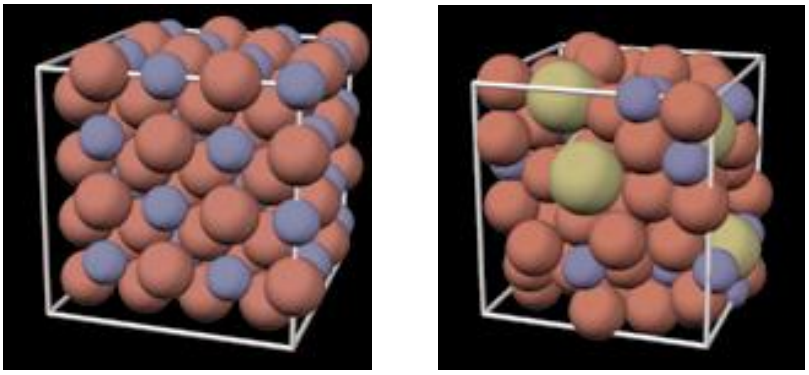

(a) (b)

Figure 3.7: Crystalline Microstructure (a), Amorphous Microstructure (b) [22]

Mechanically, the BMG exhibits high strength, large elastic strain, localized deformation with shear band, small of strain hardening, and much higher hardness than crystalline alloys of comparable elastic modulus. For example, a Zr-based BMG has 1.9 GPa tensile strength, 40-55 $MPa.m^{1/2}$ fracture toughness, and up to 2% elastic strain limit. BMG can be casted to strong thin-wall structure with precise shape. Magnetically, the iron-based BMG can be an excellent soft magnet with minimal hysterisis loss. Due to the high hardness, the BMG theoretically can exhibit excellent wear characteristics, although the wear tests show the opposite trend. Without grain boundary, the BMG has good corrosion resistance. Table 3.1 shows the comparison of the properties of Zr-based BMG with other materials

Table 3.1: Comparison of The Properties of Zr-based BMG With Other Materials.

Material	Elastic modulus (GPa)	Poisson ratio	Ultimate tensile stress (MPa)	Percent of elongation to fracture	Thermal conductivity (W/m-K)	Fracture toughness ($MPa.m^{1/2}$)
Zr-based BMG	96	0.36	1900	2	4	40 – 55
Ti alloys	110	0.34	1000	14	7.2	60
Aluminum alloy	70 – 79	0.33	100 – 550	1 – 45	177 – 237	36
Steel,high-strength	190 – 210	0.27 – 0.3	600 – 2500	2	35 – 60	50
Plastic -- Nylon	2.1 – 3.4	0.4	40 – 80	20 – 100	0.3	1

Although the BMG are very deformable, they fail in a brittle manner. The structure is amorphous, so the material cannot be strain hardened and the deformation tends to concentrate within the shear band. This deformation causes localized heating, further reducing shear resistance, and leading to thermal instability. The very low thermal conductivity of BMG, about 4 W/m-K for Zr-based BMG vs. 40-60 W/m-K for steel, hurts the conduction of heat in the shear zone and promotes the shear band formation. Therefore to improve the ductility of the BMGs, various production methods and techniques have being developed. One of them is the study of Hufnagel et al [52]. They demonstrated that increasing the Ta content from % 4 to % 8 in Zr–Cu–Ni–Al bulk metallic glass enhances the strain limit from ≈ % 4 to ≈ % 18 in uniaxial compression shown in Figure 3.8 so controlling shear band behavior in metallic glasses through microstructural design improves the ductility and toughness also.

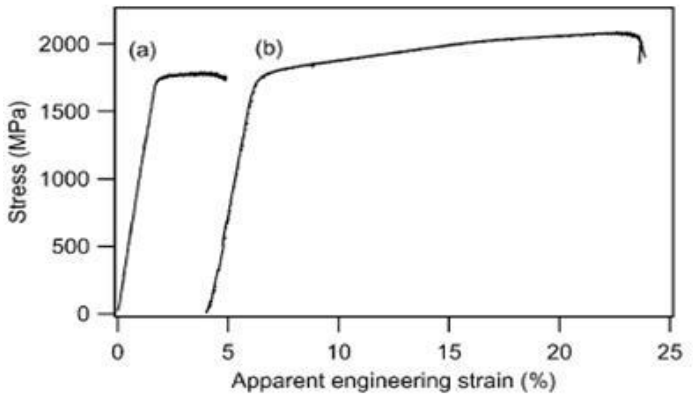

Figure 3.8: Stress–Strain Curves for Quasi-Static Uniaxial Compression for Samples With (a) a 4 at.%Ta and (b) 8 at.%Ta.

The continuous dark gray phase in Figure 3.9 demonstrates the matrix and the lighter phase is the crystalline Ta-rich solid solution.

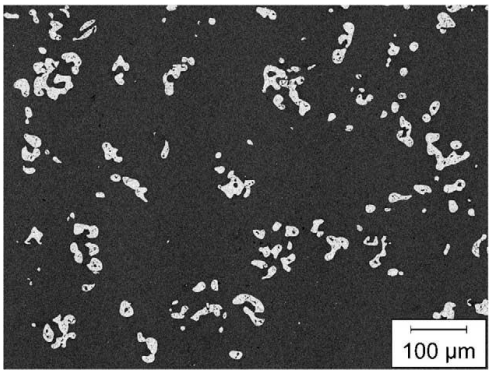

Figure 3.9: Backscattered Electron Image of $(Zr_{70}Cu_{20}Ni_{10})_{80}Ta_{10}Al_{10}$

In Figure 3.10 the crystalline particles indicated by the arrows prevent the branches of the shear band.

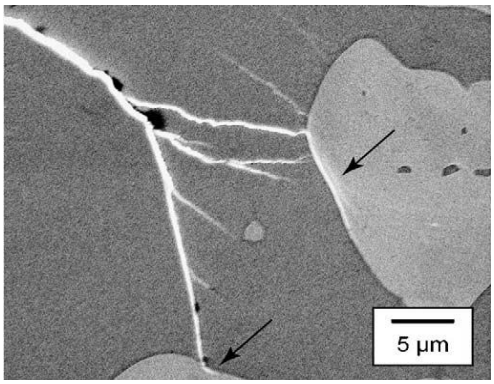

Figure 3.10: Interactions Between Shear Bands and Particles.

One of the most attractive properties of the BMGs is the mechanical strength of it. For ten years researchers have being focused on this unique property and they have developed BMGs that have fracture strength of more than 5000 MPa with 3 mm section thickness [74]. This value is very high when compared with the highest tensile strength known for a crystalline alloy which is the Fe-based alloy and used as a piano wire with a 3300 MPa tensile strength. Table 3.2 summarizes the latest developments of mechanical properties of BMG.

Table 3.2: Mechanical Properties of BMGs

MATERIAL	Thickness (mm)	Compr. Strength (MPa)	Fracture Strength (MPa)	Compr. Strain (%)	Vickers Hardness (kg/mm^2)	Young's Modulus (GPa)	Year	Refr.
Co–Fe–Ta–B	2		5185			268	2004	[75]
Fe-based BMG	4	4100	4250			215	2004	[76]
Cu-Zr	1	1860		50		104	2005	[77]
Fe–Co–B–Si–Nb	5		4250		1250	210	2006	[78]
Co–Fe–Ta–B–Mo–Si	3		5545		1693	282	2006	[78]
Cu-Hf-Ti-Nb	2	2073	2232	14.1			2006	[79]
La-based BMG	30		650		200	35	2007	[80]
Fe–Ni–Zr–Cr–Si–B	2	2000		4.03			2007	[81]
Gd-Co-Al	5		1250			63	2007	[82]
Gd-Ni-Al	4		1300			65	2007	[82]
Ni–Nb	1	3500		5.3			2007	[83]
Ni62Nb38	2		3100			231	2007	[84]
Cu-Hf -Ti -Nb	2		2625	12.5		106	2007	[85]
Ni-Nb-Zr	3	3000		1			2007	[86]
Gd-Co-A1	5	1380				70	2007	[87]
Mg-Cu-Zn-Y-Zr	2	830		2.4			2007	[88]
Cu-Zr-Ti	1.5	1680		10.6			2007	[89]
Cu-Zr-Ti	2.5	1020		18			2007	[89]
Fe-C-Si-B-P-Cr-Mo-Al-Co	6		3400	0.5			2008	[90]

3.7.1 Corrosion Resistance of BMG

It is common knowledge that crystalline alloys become resistant to corrosion due to the formation of an amorphous surface film. This knowledge suggests that metallic glasses have a good resistance to corrosion, which leads to research in this area. Several experimental techniques are being used to research corrosion of metallic glasses involving immersion tests in aqueous media.

Metallic glasses are amorphous and do not contain crystalline defects such as grain boundaries, vacancies, and dislocations. Also, the extreme cooling rates needed during production prevent significant chemical segregation. These two factors help

to induce a high corrosion resistance in metallic glasses. The amorphous structure, with few defects, provides few preferential corrosion sites. Also, the homogeneous, single-phase structure facilitates the formation of a uniform passive film, provided that protective elements are present. Metallic glasses are also highly reactive which causes corrosion resistance due to rapid passivation.

The addition of other metals to Fe, Ni, and Co based amorphous alloys leads to significant improvements in resistance to corrosion. Cr is the most effective alloying element for reducing corrosion in acidic, alkaline, and neutral environments. It is well established that Fe, Ni, and Co based amorphous alloys that have more than 8at%Cr are extremely corrosion resistant in NaCl, HCl, H_2SO_4 and $FeCl_3$ environments. The high corrosion resistance is due to the ability of Cr to form an adherent and protective hydrated chromium oxyhydroxide film [21]. The Fe-based BMGs' corrosion resistance is good enough to use them as practical corrosion resistant materials. [56]

Also, Qin et al showed that the addition of Nb to the Hf-Ti-Cu alloy provides higher chemical stability in HCI and NACI solutions and decrease corrosion rate significantly. The improvement of the corrosion resistance of the $(Cu_{0.6}Hf_{0.25}Ti_{0.15})_{90}Nb_{10}$ is attributed to the formation of Hf-, Ti-, and Nb-enriched highly protective surface films during immersion in acid- and chloride-ion-containing solutions [53,54]. Later researches by Jiang demostrated that the ion implantation technique have a remarkable enhancement of corrosion resistance in chloride containing environments and acid solution with respect to the alloy without the surface treatment while the implanted alloys still have high glass forming ability. So by this technique corrosion resistance of BMGs can be improved without losing glass forming ability and this results from the high passivating ability of the Nb-containing surface layer [55].

3.7.2 Magnetic Properties of BMG

The short range ordered structure in metallic glasses is not much different from the crystalline material and permits ferromagnetic behavior. But the magnetic properties depend on the residual strain, field heat treatment, the directionality induced during solidification, and on the composition. On average the amorphous alloys have higher permeability, lower coercivity, and higher electrical resistivity.

High coercivity of the BMGs produced in multicomponent (Nd, Pr)-Fe-based systems have attracted great attention. The reason of high coercivity is presumed to be "the precence of a relaxed disordered structure that can be regarded as an

ensemble of Nd (Pr)-Fe Nd(Pr)–Fe–Al clusters with large random magnetic anisotropy " [57-62].

Hot pressed $Fe_{67}Co_{9.5}Nd_3Dy_{0.5}B_{20}$ glassy powders in supercooled liquid state have high glass forming ability and hard magnetic properties. Hysteresis loop in Figure 3.11 shows that annealing for 600s at 913K how improve the magnetic properties of the hot pressed alloy [63].

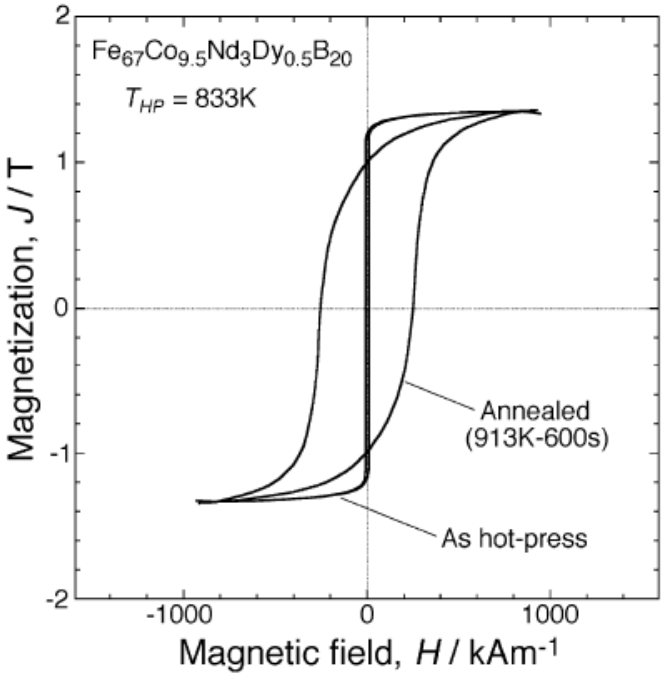

Figure 3.11: Hysteresis Loops of the $Fe_{67}Co_{9.5}Nd_3Dy_{0.5}B_{20}$ Samples in As-Pressed and Annealed (for 600 s at 913 K) States.

Also the latest researches showed that magnetic properties of fully amorphous and 6 mm diameter rods ($Fe_{68.7-x}C_{7.0}Si_{3.3}B_{5.5}P_{8.7}Cr_{2.3}Mo_{2.5}Al_{2.0}Co_x$ (x = 0 -10)) can be improved by substituting the Fe element by Co. By replacing 1–2 at% Fe by Co exhibited good soft magnetic properties [65]. Comparison of the Fe- and Co-based metallic glasses ribbons with the BMGs on account of soft magnetic properties is shown in Table 3.3 [64, 66].

Table 3.3: Comparison of The "Fe & Co Based Metallic Glass Ribbons" With BMGs On Account of Soft Magnetic Properties

Advantages and Disadvantages of BMGs on account of Soft Magnetic Properties	
ADVANTAGES	DISADVANTAGES
High electrical resistivity of 200–250 μΩ at room temperature	Higher materials cost due to the necessity of using special solute elements to obtain an higher GFA
Lower coercive force of 0.2–4 A/m;	
Higher initial permeability	
Controllable arrangement of domain wall structure achieved by control of casting and/or cooling processes	Lower saturated magnetic flux density due to the addition of large amount of solute elements
Better high-frequency permeability	
Good micro-forming ability in supercooled liquid region.	

There are three major potential applications for metallic glasses. The largest is in power devices, particularly distribution transformers. The others are transducers and magnetic delay lines, and information handling equipment [21].

4. APPLICATIONS OF BMG

BMG alloys have excellent and unique mechanical and physical unconventional properties for various applications. Up to now BMG alloy systems have already been commercialized and used as sporting goods, optical machinery parts, writing tool materials (Zr-Al-Ni-Cu, Zr-(Ti, Nb)-Al-Ni-Cu and Zr-Ti-Ni-Cu-Be) and as die materials (Pd–Cu–Ni–P) and as electrode materials (Pd-Cu-Si-P) [23]. Beside that Fe-based BMGs with soft magnetic properties will be used as common mode choke coils in near future [67].

In addition to sporting goods, the company also produces amorphous alloy products for electronic product casings, medical devices, defense applications, and industrial coatings.

Golf club heads made from BMG with low density, high strength-to-weight ratio, lower vibrational response and low elatic modulus provides better control for a golf striker. The speciality of this club is the amount of energy transferring to the ball at impact. Thanks to negligible hysteresis loss of BMG less energy absorbed by the golf club head and more energy is transferred to the ball at impact. Literature of the manufacturer of the golf club points out that the energy transferred by the club head to the ball is about 60%, 70%, and 99% of the input energy for the steel, titanium and BMG made golf heads respectively. In addition to golf clubs BMGs are also used in tennis rackets, baseball bats, and hunting bows [22].

On the other hand, size of the electronic appliances such as MP3 players and mobile phones are reducing day by day and there is a need to produce thinner cases with sufficient mechanical strength. So BMGs with unique properties compensate market needs and are used as casing materials of mobile phones and digital cameras [22].

Military is another application area of the BMGs. To prevent the biological toxicity of the current depleted uranium penetrators, new BMG made tank-armor penetrators have being developed instead of it [22].

Since it is highly biocompatible and non-allergic BMG is also an ideal material for medical components such as prosthetic implants and surgical instruments. For instance knives for opthomology were developed to facilitate cataract surgery.

LVMH began working with BMG technologies to develop a watchcase for LVMH's premium TAG Heuer brand. BMG alloy has 2.5 times the strength of commonly used titanium alloys and 1.5 times the hardness of a commonly used stainless steel, making it ideal for luxury watchcases. BMG alloy combines the processing and net-shaping advantages of plastics with performance characteristics that exceed in many respects those of titanium and stainless steel, allowing for unique sophisticated designs such as watchcases. Possible applications of the BMGs are presented in the Table 4.1.

Table 4.1: Possible Applications of BMG

Applications	Technical Properties
Golf Clubs [C]	High strength
Corrosion resistance materials	High corrosion resistance
Edges for Sport Goods (skies, skates)	High hardness, wear and corrosion resistance, ability to be sharpened
Bonding materials	High fatigue strength
Soft magnetic materials	Good soft magnetism
Die materials	High fracture toughness
Armacor Coating [C] (Liquidmetal)	High wear, temperature and corrosion resistance
Wires for Musical Instruments	High strength, hardness, wear and corrosion resistance, castability, abilities for surface finishing
Jewelry (Pd- Pt based alloys)	High strength, high workability
Machinery Structural Material	High hardness, wear and corrosion resistance, precious metal content, high workability
Machinery structural materials	High strength
Cutting materials	High hardness
Knives for Ophthalmology [C]	High hardness, wear and corrosion resistance
Tool materials	High impact fracture energy
Sporting goods materials	High elastic energy
Materials for Digital Master Discs	Wear resistance, no grain structure
Writing appliance materials	High wear resistance
Optical precision materials	High reflection ratio
Hydrogen storage materials	High hydrogen storage
High magnetostrictive materials	High frequency permeability
Electrode materials	Efficient electrode
Composite materials	High viscous flowability
Acoustic absorption materials	High acoustic attenuation
Penetrator	Self-sharping property
Medical devices materials	High wear resistance and manufacturability

[C]: Commercialized Products

4.1 Industrial Coatings

Alloy coatings used in industrial equipment and machinery provide the benefits of an amorphous surface in tough environments of high wear, temperature and corrosion. These coatings will significantly extend part life. From the wall of a refinery coker, to the firebox of a 1500MW utility boiler, to drill pipe exploring for oil thousands of feet beneath the sea floor, industry relies on metallic glass coatings to provide dependable, economical solutions to equipment wear. Figure 4.1 shows abrasion test results of BMG made Armacor.

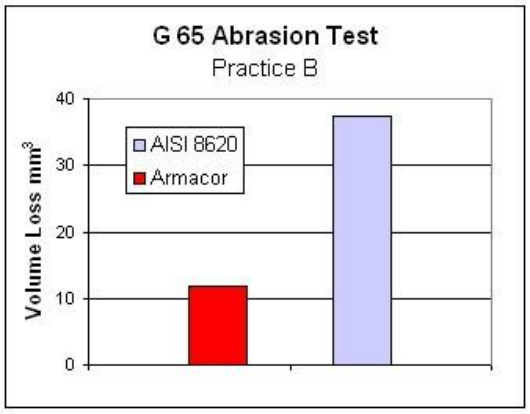

Figure 4.1: Abrasion Test Results of The BMG With A Conventional Metal

Some of the benefits are:

- Lowest coefficient of friction of any metallic coating
- Superior bond strengths without the use of bond coat
- Withstands repeated thermal cycling
- Excellent hardness at elevated temperatures
- Excellent thermal conductivity
- Application via twin wire arc spray at 25 lbs./hour
- Hardness exceeding all other sprayable wires
- Maintain tube systems on-site avoiding high replacement costs

4.2 Defense Applications

Including metallic glass alloys in a wide range of military products could significantly enhance the performance and safety levels of these products. The initial military product identified was the KEP, the most effective armor piercing ammunition used by the military. Since the KEP utilizes Depleted Uranium (DU) alloy KEP rods, the Department of Defense is searching for a new environmentally safe KEP material that performs as well as DU. Based on initial testing, the Army found the BMG refractory based alloy composite has unique characteristics that make it an improved material for use as KEP rods in advanced armor-piercing ammunition. As a result, the Department of Defense is working closely with BMG Technologies to develop a range of KEP rods that is suitable to replace current DU rods. Figure 4.2 shows an application of BMG as a defense application on armored tanks.

Figure 4.2: There is An Application of BMG Made KEPs as A Defense Application

The properties of metallic glass alloys making them suitable for the defense projects are:

- Very high yield strength
- High hardness
- High specific strength
- Very high elastic limit
- Very good corrosion resistance
- Low thermal conductivity
- Near net-shape casting
- Formed from bulk shapes or coatings

4.3 Electronic Product Casings

The revolutionary performance and processing characteristics of metallic glasses create a unique opportunity to provide innovative design and manufacturing solutions to the electronics and telecommunications equipment manufacturing industries. Metallic glass alloy allows manufacturers maximum design flexibility to produce stronger casings that are both smaller and thinner. Recent performance and processing tests with major manufacturers reveals, metallic glass is, in many cases, a superior alternative to magnesium, aluminum and titanium in manufacturing casings for electronic products and cell phone casings. The amorphous alloy combines the processing and cost advantages of plastics with performance characteristics that exceed in many respects those of titanium and magnesium. Figure 4.3 shows an application of BMG as a casing material for electronic product.

Figure 4.3: There is An application of BMG as A Casing Material for A Mobile Phone

- Produce thinner, smaller and stronger casings for electronic products and cellular handsets
- Processing advantages comparable to plastics provide revolutionary solutions to current miniaturization concerns with electronic and cellular casings
- Processed more easily than any other super alloy, it can be readily fashioned into intricate, innovative designs resulting in a unique aesthetic advantage

- With approximately 2.5 times the strength of a commonly used titanium alloy and 1.5 times the hardness of a commonly used stainless steel, metallic glasses can enable sophisticated, engineered designs required by the evolution of new technologies such as 3G
- Offer low thermal, magnetic and electrical conductivity which provides shielding from potentially harmful electro-magnetic fields

4.4 Medical Devices

Products can now be developed for use in the medical fields with better performance results than the existing devices. One of the initial areas taking advantage of the metallic glass technology is in the field of ophthalmic surgery, where procedures are being enhanced to better serve patients in need of cataract surgery.

Metallic glasses can yield knives that are:

- Sharper than steel
- Less expensive than diamond, and higher quality
- More consistently manufactured than steel or diamond
- Lower edge degradation with use
- Longer lasting blades that yield more consistency in the final product

Another opportunity is in the orthopedic field in areas such as reconstructive devices, fracture fixations, spinal implants and instrumentation.

4.5 Sporting Goods and Leisure Products

This revolution in materials science will soon be found in the forefront of design centers throughout the world, with measurable performance benefits never before realized. Potential manufacturing opportunities include golf club components, skis, baseball bats, ice skates, tennis rackets, bicycles and scuba equipment, to name only a few.

Taking advantage of a revolutionary class of a next generation super alloy that was originally launched in golf clubs in 1998, metallic glass companies are now moving on and expanding their presence to the sporting goods arena. The prolific launch of metallic glass in sports allowed scientists and engineers to better understand the properties of the alloy as it relates to a variety of sporting/leisure industry equipment needs. Figure 4.5, shows an application of BMG as a sporting good.

Some of the characteristics making metallic glasses ideal for high-performance sporting goods are:

- Nearly 3 times the strength of its counterparts
- 2-3 times higher in resistance to permanent deformation than conventional metals
- Ideal mid-range density between titanium and steel
- Excellent inherent low frequency vibration damping
- Non-corrosive
- 3-4 times as elastic as comparable super metals
- Nearly twice the hardness of stainless steel and titanium

4.6 Space Projects

Due to metallic glass alloy's extraordinary performance characteristics, NASA has been working on numerous shuttle missions for the NASA scientists to study its technology first hand in space. It has already been a part of four space shuttle missions, with scientists testing effects on the alloy in micro-gravity conditions. Because of its extraordinary performance characteristics, the glass alloy is also being considered for several upcoming aerospace applications. Currently, NASA's Genesis spacecraft, the first mission to collect and return samples of the solar wind, is continuing its trek toward the sun. BMG alloy based solar wind collector tiles, about the size of a coffee cup lid, will play a key role in the collection process. The mission is designed to measure the composition of isotopes in solar matter. The spacecraft, with its onboard experiments, is scheduled to return to earth in 2003. Figure 4.4, shows an application example of BMG at Space projects.[22]

Figure 4.4: There is An Application Example of BMG at Space Projects.

4.7 Fine Jewelry

One of the latest industries to discover the unique and innovative qualities of Liquidmetal® alloys is the fine jewelry industry. Liquidmetal alloys are essentially "metallic glass" and can achieve a stunning surface finish that is attracting the attention of high-end jewelry makers worldwide. The revolutionary properties of Liquidmetal alloys also provide strength, processing and finishing advantages never before possible with other high-performance metals. Among the qualities Liquidmetal alloys offer the jewelry industry are:

- Timeless lifecycle due to superior hardness and scratch resistance
- Precision net-shape casting capability
- Ability to be polished to a luxurious finish
- Strength-to-weight twice that of titanium
- Approximately 2-3 times the strength of traditional metals used in jewelry
- Ambient room temperature feel
- Dent and corrosion resistance

The key to these high-performance characteristics is the ability of Liquidmetal alloys to retain a random, or "amorphous" atomic structure during solidification, unlike other metals which "crystallize" when they transition from molten to solid form. This creates a metal surface that is both exceptionally hard and scratch resistant, but can be polished to a high luster that is maintained over time. Also, the ability of Liquidmetal alloys to be precision net-shape cast enables jewelry designers to create bold lines and sensual, unique shapes not easily achieved with traditional metals.

4.8 Hinge Applications

The latest application developed for Liquidmetal alloys is in the field of hinge components for electronic housings in the mobile phone industry shown in Figure 4.5. With the increased complexity in handset circuitry, a greater demand is placed on the performance of internal structural components. As a result, the use of conventional materials becomes inadequate to meet the new performance benchmarks.

Liquidmetal alloys are ideally suited for critical-performance applications where close manufacturing tolerances are vital. Cell phone hinge housings represent a perfect example of critical performance needs where incumbent materials such as zinc, magnesium, stainless steel and even titanium have inherent design and

performance limitations. Hinge components made with other lower-strength metals have less resilience to impact from dropping or the daily wear-and-tear of repeated flip-phone actions. On the other hand, Liquidmetal alloys have superior yield strength and elasticity, properties that resist deformation and provide exceptional durability. In addition, structural parts made from Liquidmetal alloys can be net-shape formed to thinner profiles while maintaining their superior strength, resulting in more design space to accommodate consumer demands for new technology.

Key Liquidmetal alloys advantages for hinge components include:

- Reliability for repeated load-bearing conditions
- Flexibility of design to meet customer needs
- Much higher yield strength & hardness greater than any commercially cast alloys
- More room for FPCB design and accommodation
- High dimensional accuracy and stability
- Outstanding surface finish with near net shape casting process
- Superior corrosion resistance

Figure 4.5: Application of BMG As Hinge Material on Mobile Phones

Liquidmetal alloys also provide both a competitive price-performance combination and a quick development cycle using a concurrent engineering process, leading to a large production capacity with high quality control.

Liquidmetal alloys hinge application represents the launching point for a wide range of similar niche categories that will benefit from the strength and performance advantages of Liquidmetal alloys

5. EXPERIMENTAL STUDY

5.1 Experimental Setup

All drilling and milling experiments were conducted in a Spinner VC 650 computer numerical controlled machining center shown in Figure 5.1 (a). A piezoelectric force dynamometer "Kistler 9257B" shown in Fig 5.3 and Fig.5.2 (a) and a National Instruments 6036E DAQ card and a BNC2120 board shown in Figure 5.1 was used to measure the cutting forces during tests. The force data was acquired with "CutproV8" and processed with Matlab softwares. By using a JEOL 7000F SEM, chip morphology and burr formation were examined. MahrSurf XCR29 model surface roughness measuring instrument was used to measure the surface roughness of the holes. An infrared thermal imager "IRI4010" shown in Figure 5.2 was used to measure the maximum temperature of the material during the cutting.

(a) (b)

Figure 5.1: Spinner Machine Tool (a) BNC2120 and Control Unit of Dynomemeter (b)

(a) (b)

Figure 5.2: Thermal Imager (a) Kistler Dynamometer 9257B (b)

5.1.1 Experimental Design of Drilling

By using a set screw shown in Figure 5.3 (b) inside a support plate, 6.35 mm diameter 2 mm thick disk workpiece was fastened. All of the drilling tests were conducted dry without using coolant.

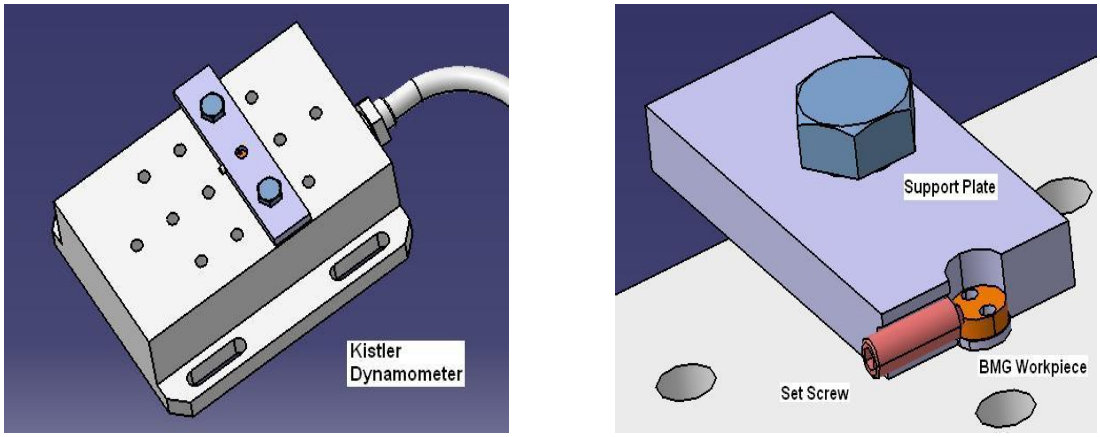

(a) (b)

Figure 5.3: Experimental Setup; (a) Configuration of Drilling Test and (b) Schematic Representation of The Disk Workpiece Hold by The Set Screw Inside a Support Plate.

The tool-materials were DIN 338 MICROGRAIN WC RN 118° and TiAlN coated WC in cobalt matrix denoted as MG-WC and WC, respectively. Light emission during drilling was recorded but no light emission was observed.

5.1.2 Experimental Design of Milling

By using a small vise shown in Figure 5.4, 6.35 mm diameter 2 mm thick disk workpiece was sequeezed between the clamps. All of the milling tests were conducted dry without using coolant.

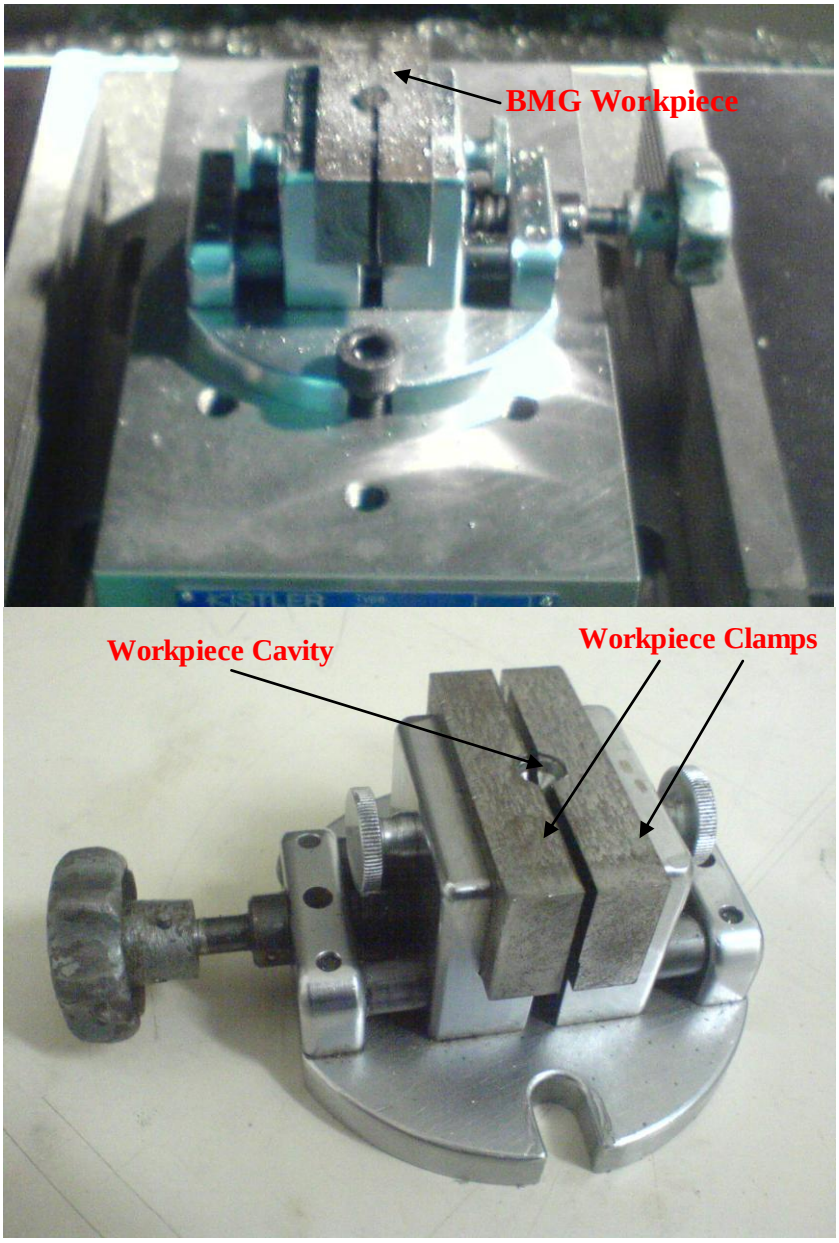

Figure 5.4: Workpiece Holding Equipment for Milling Tests

The tool-materials were WC and HSS and all the end mills are uncoated.

5.2 Drilling

Drilling is a widely used machining process in various industries for hole making. A typical twist drill shown in Figure 5.5 is complicated because of several design parameters (helix angle, chisel edge angle, cutting length, tip angle) and changing cutting speed along the cutting edges during drilling. Also rake angle changes along the cutting edge and becomes equal to helix angle at the outer corner of the cutting edge. The majority of thrust force formed during the drilling is produced by cutting edge. In addition to tool geometry, workpiece material, process parameters (feed rate, spindle speed) and vibration of machine tool effect the hole quality [23,24].

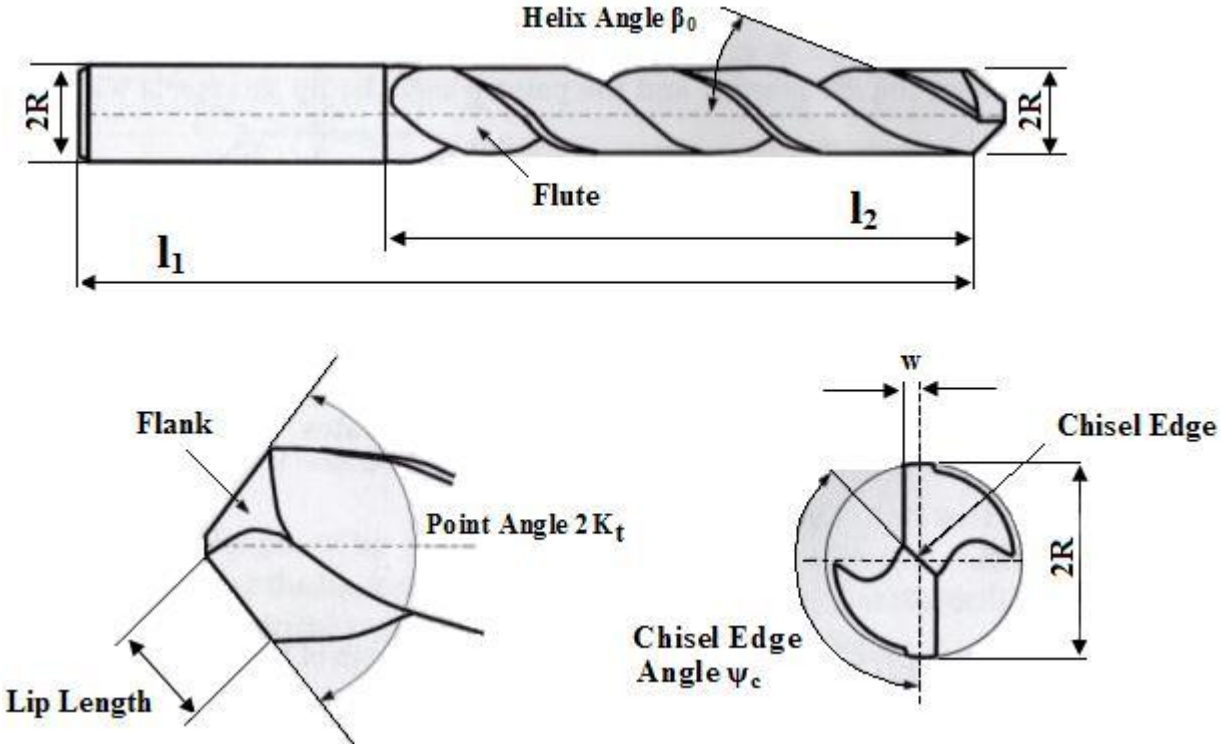

Figure 5.5: Twist Drill

Three sets of drilling experiment, marked as Exp 1-4 were conducted. In the first two sets of experiment (Exp. A-B) effect of tool material and feed rate are investigated. In Exp. C, work material effect is investigated.

Exp. A. Feed rate effect: 1, 2 μm/rev feed rate for 2 mm diameter MG-WC drill at 2500 rpm spindle speed.

Exp. B. Tool Material Effect: WC drill with 2 mm diameter at 2500 rpm and at 1 and 2 μm/rev feed rate (compared to MG-WC drill in Exp. A).

Exp. C. Work Material Effect: SS304 workpiece is drilled using a 2 mm diameter MG-WC drill at 2500 rpm and 0.1 and 0.2 μm/rev feed rate (compared to BMG material drilled in Exp. A).

Table 5.1: BMG Drilling Process Parameters, Chip Formation and Burr Quality

Exp.	Workpiece Material	Drill Material (mm)	Drill Diameter (mm)	Feed Rate (μm/min)	Spindle Speed (rpm)	Work Material	Chip Morphology [a]	Exit Burr Quality [b]
A	BMG	MG-WC	2	1 2	2500 2500	BMG	# 2 Snarled # 2 Snarled	1 0
B	BMG	WC	2	1 2	2500 2500	BMG	# 1 Snarled # 1 Snarled	0 0
C	SS304	WC	2	1 2	2500 2500	SS304	# 1 Long # 2 Long	0 0

[a] Type of chip -- # 1, Ribbon; # 2, Helical.

[b] Exit burr quality – 0, visible burr; 1 not visible burr

5.2.1 Thrust Force Analysis

Table 5.2 shows the thrust force results for same process conditions (2,500 rpm spindle speed, 0.1 and 0.2 μm/rev feed rate for BMG. For the sake of comprison, solid and micrograin carbide tool result for BMG also presented in same graph. Force diagrams of drilling tests are shown in Figure 5.6 (a) (b) (c) (d).

Table 5.2: Thrust Forces for Different Feed Rates and Tool Materials.

Tool Material		HSS	Solid WC	Micrograin WC
		F_t [N]	F_t [N]	F_t [N]
	f [μm/rev]			
BMG	0.5	65-70	30-40	50-60
	1	-	~ 40	70-80
	2	-	~ 50	~ 80
	6	-	~ 70	100-120

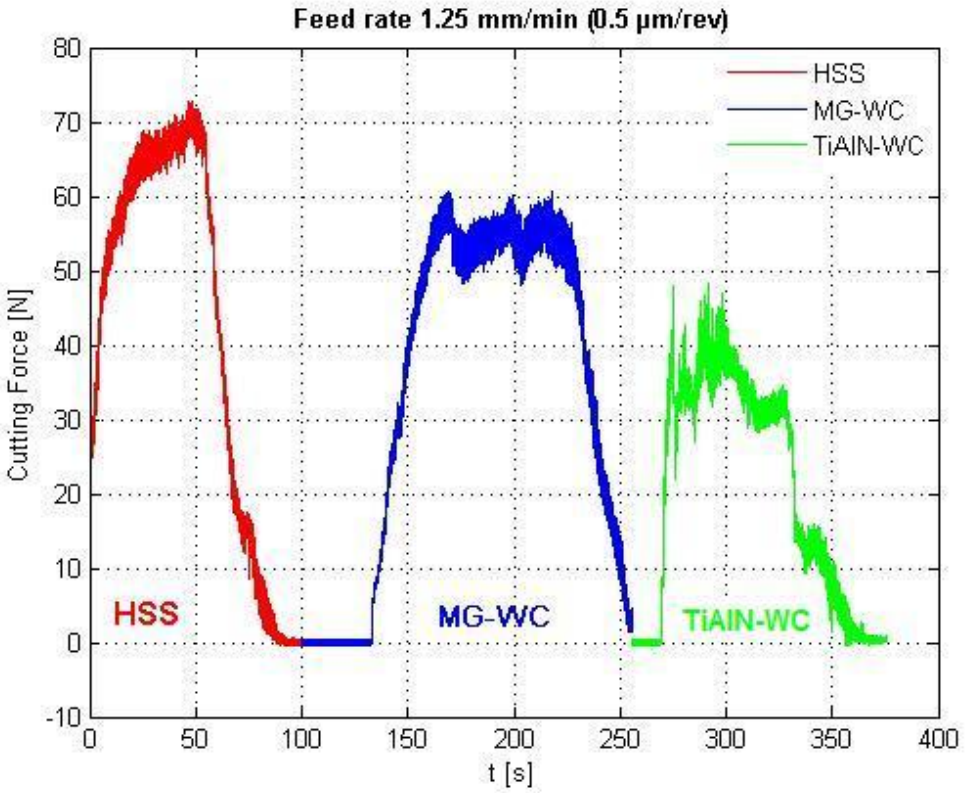
Feed rate 1.25 mm/min (0.5 µm/rev)
HSS
MG-WC
TiAlN-WC
Cutting Force [N]
t [s]
HSS
MG-WC
TiAlN-WC

(a)

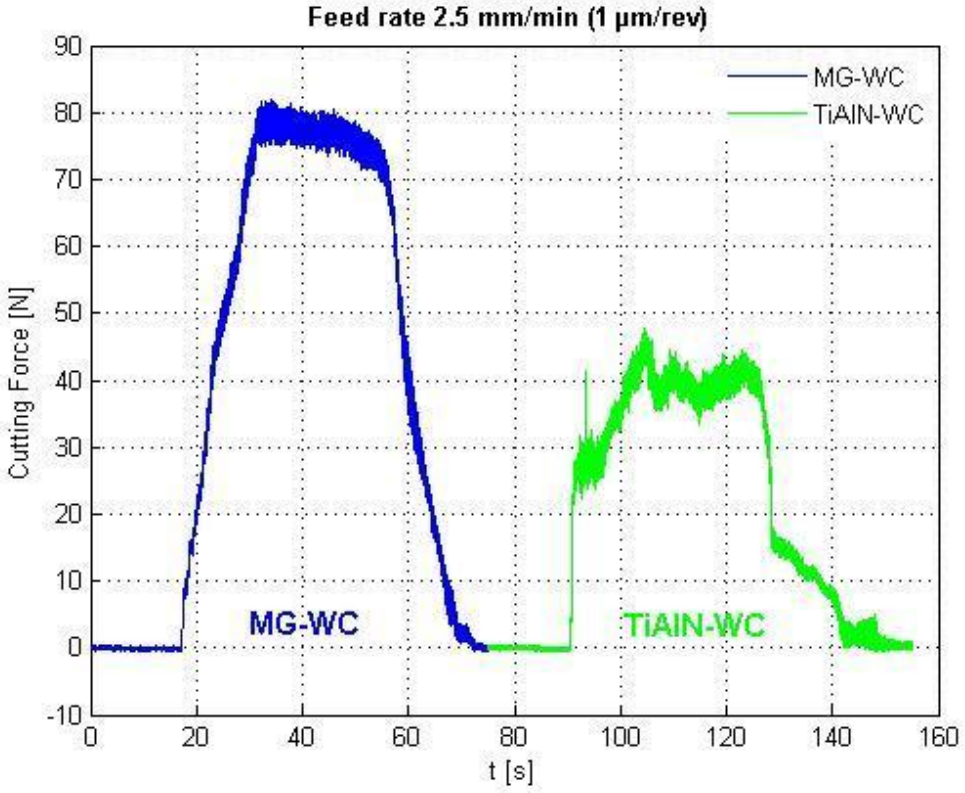
Feed rate 2.5 mm/min (1 µm/rev)
MG-WC
TiAlN-WC
Cutting Force [N]
t [s]
MG-WC
TiAlN-WC

(b)

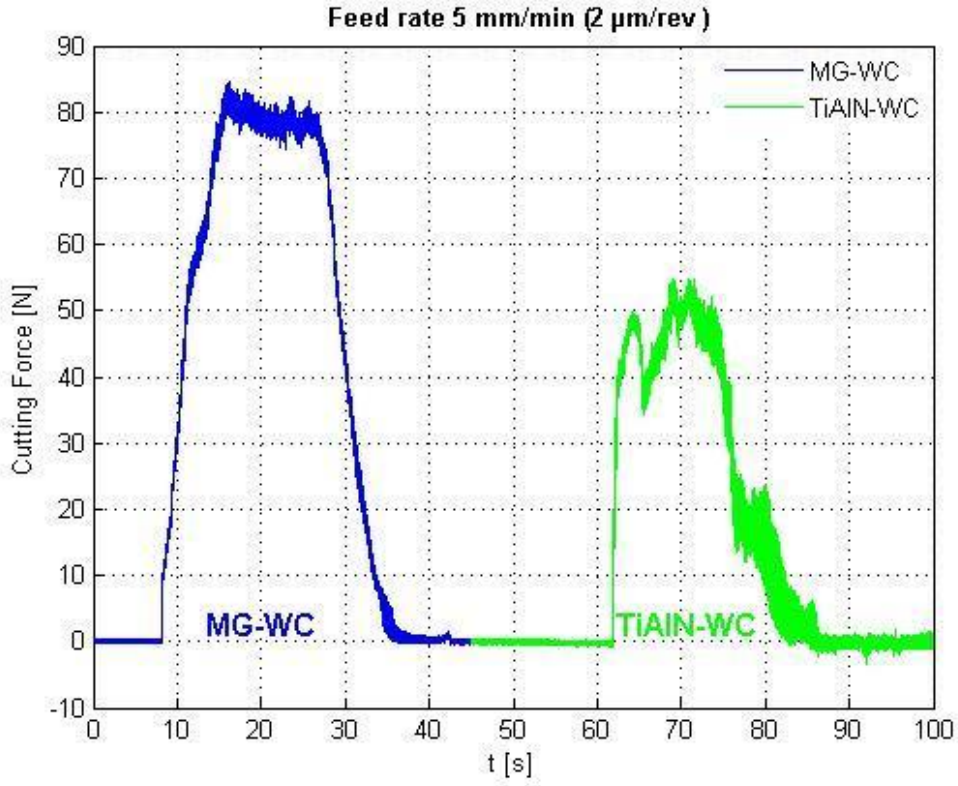

(c)

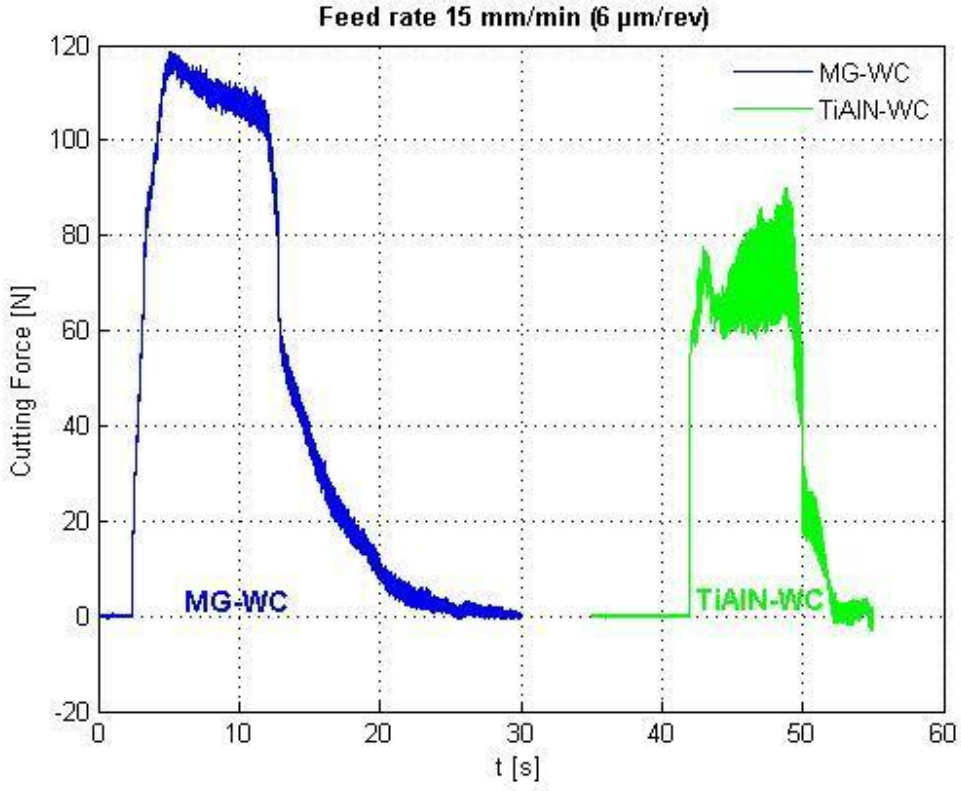

(d)

Figure 5.6: Thrust Force Diagrams of Drilling

Effect of feed rate is obvious for both tool materials. Higher thrust forces can be seen at higher feed rates. Increase on thrust force value is about 30 percent more when two times higher feed rate on BMG is applied.

Results show that under the same drilling conditions HSS tool required the most thrust force at 0.5 μm/rev and was broken at feed rates higher than 0.5 μm/rev. The micrograin carbide tool, submicron size carbide grains in it, generally requires more thrust force than coated one.

5.2.2 Chip Morphology

Chip morphology plays an important role in machinability. Due to process parameters, work and tool materials and drill geometry, chip morphology varies in size and shape. According to ISO-based chip-form classification, long spiral snarled and long ribbon snarled type chip morphology of BMG is observed in this study. These long and snarled chips wrap the tools completely as shown in Figure 5.7.

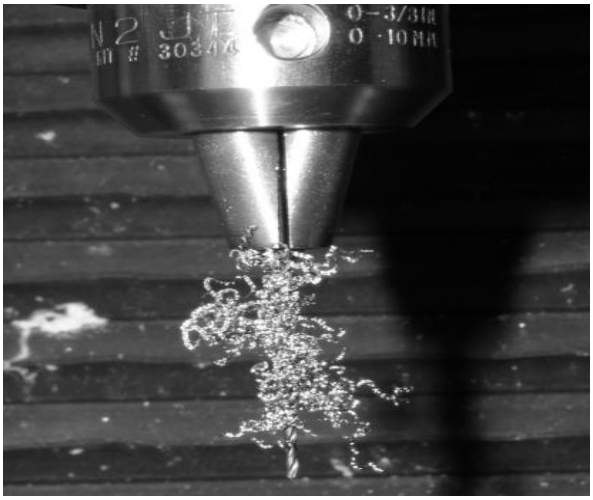

Figure 5.7: Tangled Chips Around Carbide Drilling Tool at 2 μm/rev (5 mm/min) Feedrate.

- **Ribbon Shape Snarled Chips**

Solid and MG-WC tools were produced similar, ribbon shape snarled chip morphology, at 1 μm/min feed rate for BMG drilling. Both chip morphologies are presented in Figure 5.8 and Figure 5.9 at three magnification level. Cracks on both sides of the ribbon chips due to extrusion in the drill center wedge and high cutting speed on the outside cutting edge can be seen on both chip micrographs.

The effect of tool material on chip morphology is revealed by comparing Figure 8,9. As it can be clearly seen at Figure 8(c) and Figure 9(c), solid WC tool creates more significant shear bands on chip surface than that of MG-WC tools.

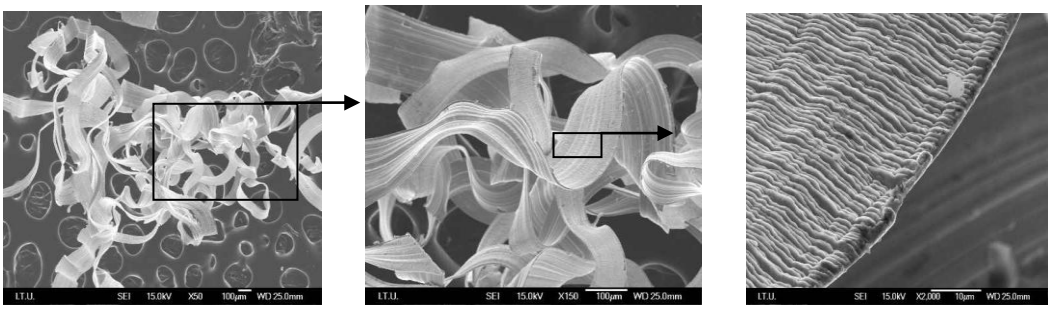

(a) (b) (c)

Figure 5.8: Ribbon Shape Snarled BMG Chip in Exp. A; 1 μm/min Feed Rate (a) General View, (b)Close-Up View of The Box in (a) Shear Bands on The Chip Surface

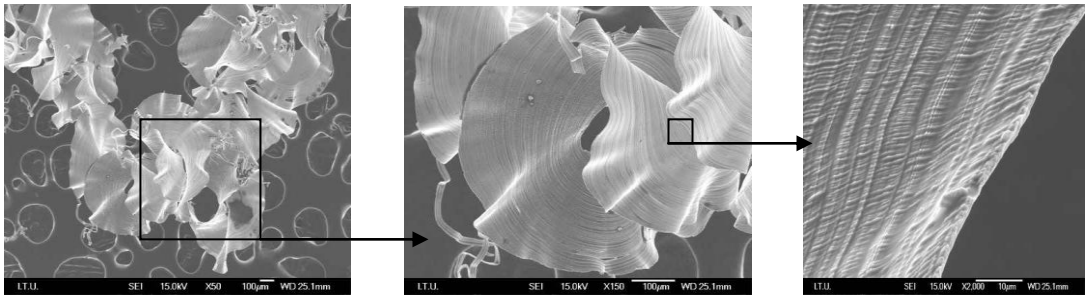

(a) (b) (c)

Figure 5.9 Ribbon Shape Snarled BMG Chip in Exp. B; 1 μm/rev Feed Rate (a) General View, (b)Close-Up View of The Box in (a) Shear Bands on The Chip Surface.

- **Helical Shape Snarled Chips**

Detailed views of helical shape snarled chips generated in Exp. A and B at 2 μm/rev feed rate is shown in Figure 5.10 and 5.11 at three different magnification. There are sign of cracks on both sides of the ribbon chip on solid carbide tool used tests. Micrograin carbide tools create more clear chip morphology at higher feed rates. According to difference between chip morphologies clearly offer that micrograin carbide drilling tools are more suitable for BMG drilling at higher feed rates. These results also confirmed with created less exit burr formation (Figure 12(b)) and significantly lower surface roughness with micrograin carbide tools.

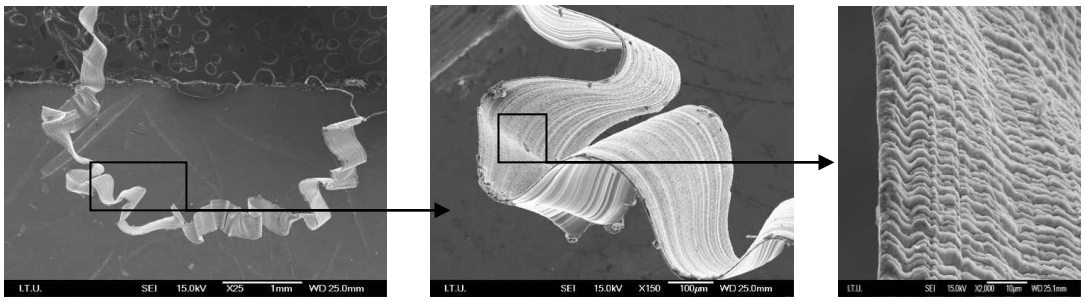

(a) (b) (c)

Figure 5.10: Long Spiral Snarled BMG Chip in Exp. A; 2 μm/rev Feed Rate (a) General View, (b)Close-Up View of The Box in (a) Shear Bands on The Chip Surface.

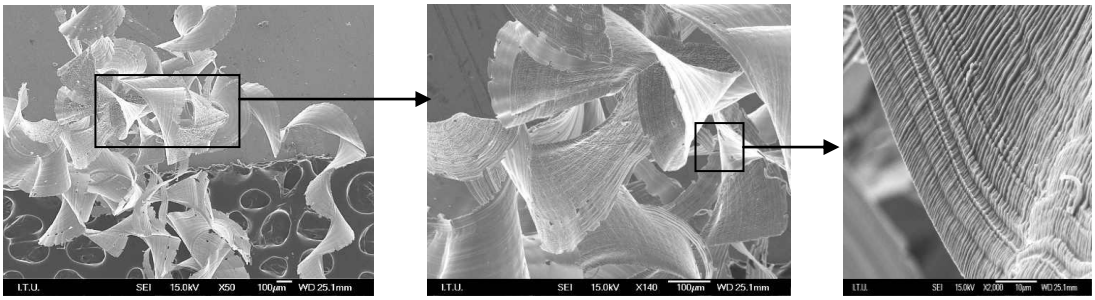

(a) (b) (c)

Figure 5.11: Long Ribbon Snarled BMG Chip in Exp. B; 2 μm/rev Feed Rate (a) General View, (b) Close-Up View of The Box in (a) Shear Bands on The Chip Surface.

5.2.3 Burr Formation

Burrs are thin ridges and usually develop along the edges of a workpiece from machining. If the burrs intercede with the assembly of parts they can cause misalignments, jamming of parts and short circuits in electrical components. In this study burr formation was observed in the exit edges of the drilled BMG holes. There was no evidence on entrance burr in BMG parts. In Figure 5.12 (a), (b), and Figure 5.13 (a), (b) SEM micrographs of the MG-WC and solid WC drill used exit burrs are shown, respectively. Crown shaped exit burr can be seen clearly for lower feed rate drilling with micrograin WC tool and both feed rate for solid WC tools. As seen from the Figure 12 (b) there is almost negligible burr formation produced at 2 μm/rev feed rate with micrograin WC tool.

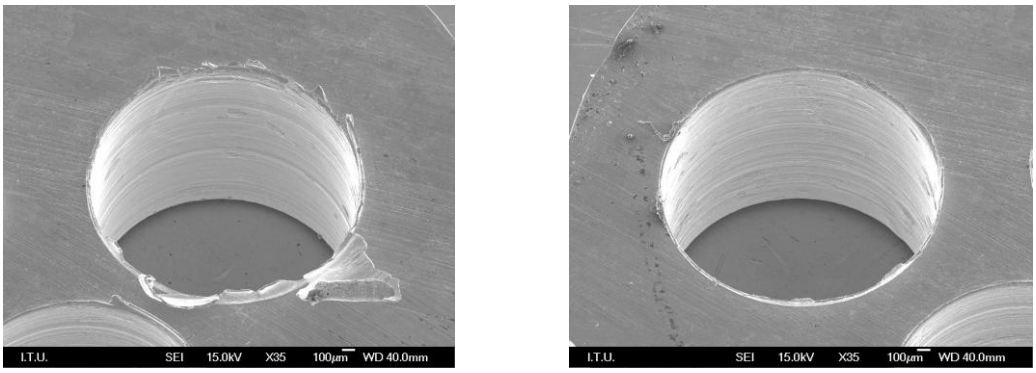

(a) (b)

Figure 5.12: Exit Burrs in BMG Drilled by Micrograin WC in Exp. A (a) 1 µm/rev (b) 2 µm/rev Feed Rate.

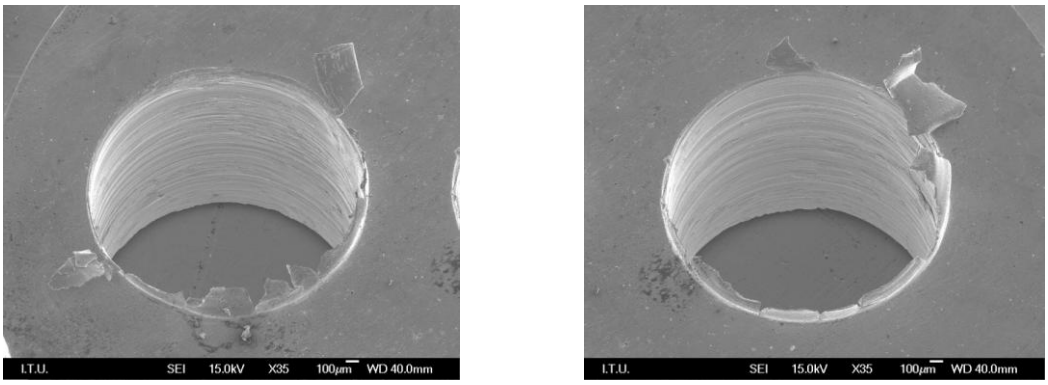

(a) (b)

Figure 5.13: Exit Burrs in BMG Drilled by Solid WC in Exp. B (a) 1µm/rev (b) 2 µm/rev Feed Rate.

5.2.4 Surface Roughness

The measurement of surface roughness is among important aspects of manufacturing. Surface of a material affect the materials corrosion, fatigue, wear, friction, thermal and electrical conductivity. In this study surface roughness of the holes drilled in Exp A and B as shown in Table 5.3 were measured by using a profilometer. Results present that micrograin WC tool provides better surface roughness than that of solid WC tool under the same process conditions. Each result in the Table 5.3 was calculated by taking the average of three measure of profilometer. Results of surface measurement offers that 2 µm/rev feed rate creates better surface roughness than that of 1 µm/rev feed rate for both drill material (Figure 5.14 & 5.15). In addition to that same results confirm those MG-WC tools are more suitable for BMG drilling at 2500 rpm. Resultant surface roughness values for drilling are in the range of grinding process roughness range [24]. This result shows that it is easy to get good surface finish in BMG parts even with conventional machining processes.

Table 5.3: Surface Roughness Values of BMG

Tool Material	Feed Rate (μm/rev)	R_a (μm)	R_z (μm)	R_{max} (μm)
Micrograin WC	1	0.375	2.16	3.28
Micrograin WC	2	0.172	0.98	1.40
TiAlN-WC	1	0.873	4.88	7.83
TiAlN-WC	2	0.418	2.49	3.49

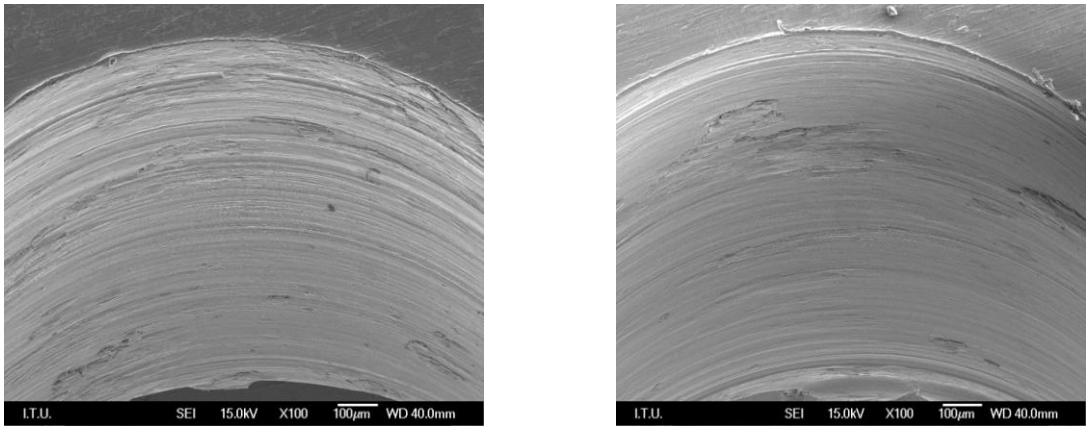

(a) (b)

Figure 5.14: Surface Views of BMG Drilled by MG-WC Tool at (a) 1 μm/min (b) 2μm/min Feed Rate.

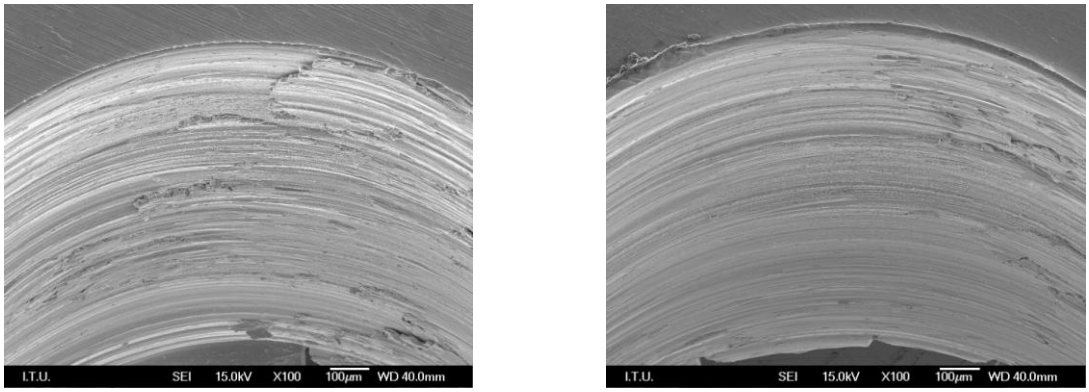

(a) (b)

Figure 5.15: Surface Views of BMG Drilled by Solid WC Tool at (a) 1 μm/min (b) 2 μm/min Feed Rate.

5.3 Milling

Milling is one of the most widespread processes used by producers in the industry to produce complex parts and molds with high dimensional accuracy and surface quality. The clamped workpiece on the table is linearly moved toward a cutterheld in a rotating spindle and the material is removed from the clamped workpiece by a rotating cutter which has one or more teeth. Peripheral milling and face milling are the two basic milling operations. The difference between these operations is the direction of the rotation axis according to generated surface shown in Figure 5.16. In peripheral milling (or plain milling) the axis of rotation is parallel to the generated surface but in face milling it is perpendicular [68].

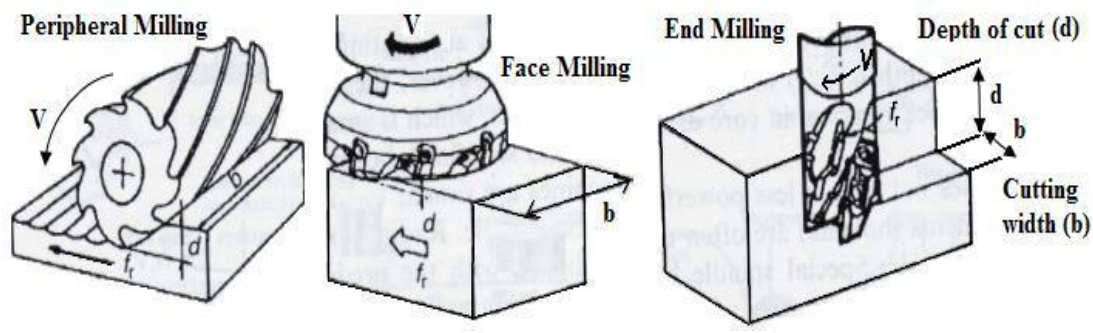

Figure 5.16: Milling Types [68]

In end milling operations the axis of rotation is both parallel and perpendicular to the generated surface. So end milling is also a type of peripheral milling operation. In milling processes the entry and exit angles of the rotating cutter determines the milling operation whether up milling or down milling. In up milling operations, the entry angle of cutter is zero and the exit angle is nonzero but in down milling operations the entry angle is nonzero and the exit angle is zero. In particular applications both up and down milling operations have advantages. If the surface of the workpiece is hardened due to sand casting or flame cutting or the dimensional variations in height are large on the part up milling operation is preferred. In peripheral down milling, cutting forces tend to hold the workpiece on the table and reduce cutting vibrations if the spindle and feed drive don't exhibit backlash.

Depending on the workpiece geometry, there are various kinds of tools, tool holders and machine tools used in milling operations. In this project, all milling experiments were made by using helical end mill.

In this study helical end mills were used during the machining operations. Therefore mechanics of helical end mills is examined in this section.

5.3.1 Mechanics of Helical End Mills

Since the cutting forces are periodic and stimulate oscillatory vibrations, simulation of milling is more diffucult than other machining operations like turning and boring. To optimize the cutting conditions and tool path in end milling operations Klein's well-known model [69, 70] is reviewed in this section.

To dampen the mechanical and thermal stresses caused by the periodic loads, helical end mills are used. The walls of the workpieces machined by helical end mills are the target finish surfaces in peripheral milling. A typical helical end mill is shown in Figure 5.17 [25]. To understand the mechanics of end mills it is obligatory to know the geometry of helical end mills. As shown in the Figure 5.18 [68], chip load along the helical flutes increase gradually and if the cutter has a nonzero helix angle, a point on the axis of the cutting edge will be lagging behind the end point of the tool.

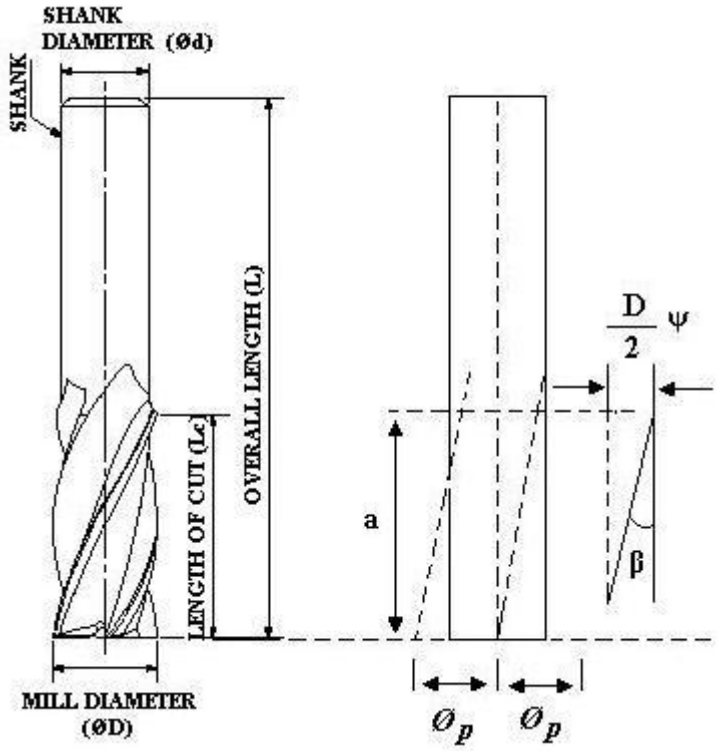

Figure 5.17: Geometry of Helical End Mill

For a given depth of cut, the lag angle is calculated from the formula below:

$$\tan\beta = \frac{D\psi}{2z} \quad , \quad \psi = \frac{2z\tan\beta}{D} \tag{5.1}$$

The immersion angle of a cutting edge point above z [mm] from the bottom surface will be (ϕ-ψ) for an immersion angle ϕ at the bottom point of a reference flute. Obviously, the chip thickness also will be different along the flute's axis.

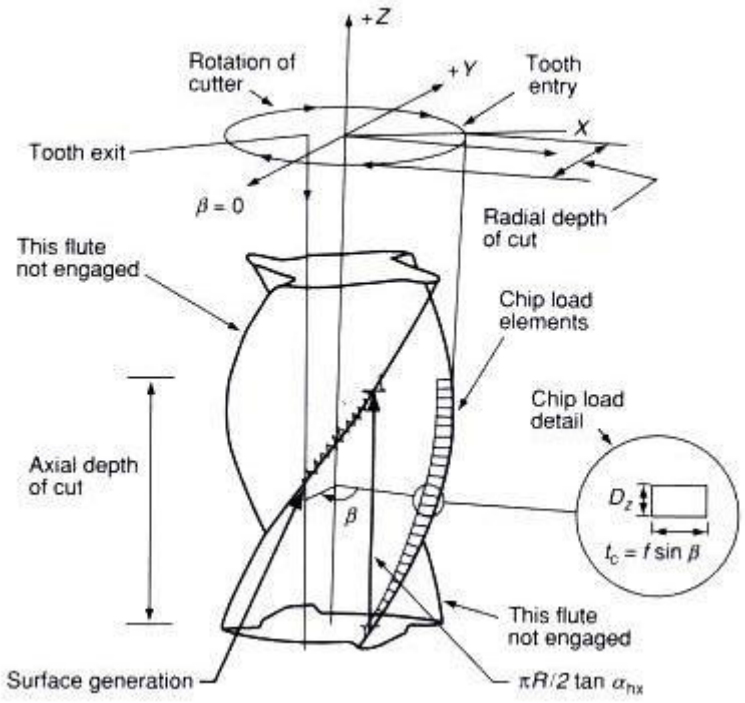

Figure 5.18: Uncut Chip Areas Along The Cutting Flute

5.3.2 Analytical Modeling of End Milling Forces

Existince of high cutting forces during milling operations can cause workpiece and tool deflections, tool breakages, chatter vibrations and machine tool damages. These widespread reasons reduce productivity, precision and part quality in various milling operations. To solve these issues or reduce their effects is possible by modeling the milling processusing a static analysis.

The critical factor which determines the accuracy of the cutting force prediction is the selected digital integration interval. For a long axial depth of cut, a small differential height must be chosen to avoid numerical oscillations on the cutting force wave forms. Also the prediction of dimensional form errors left on the machined surface depends on accurate prediction of force distribution along the end mill and flexible thin webs.

For a given cutter geometry, cutting conditions and work material periodic milling forces can be modeled and simulated. The milling force components for an up millig operation are shown in Figure 5.19. In the peripheral milling operations, the x axis is parallel with the feed direction and the y axis is perpendicular with the cut surface.

Cutter immersion angles into the workpiece, axial depth of cut, tool geometry, feed rate, spindle speed and direction of rotation determines the cutting forces and chip generation.

For an end mill with a helix angle of β, diameter of D and N number of flutes are the known parameters from the cutter geometry. Beside that, the constant axial depth of cut and the immersion angle which is measured clockwise from the normal (y) axis are the user defined parameters. The bottom end of one flute is designated as the reference immersion angle ϕ.

The lag angle is $\psi = k_\beta z$ (5.1) and the immersion angle for flute j also $\phi_j(z) = \phi + j\phi_p - k_\beta z$ (5.2) at an axial depth of cut z.

The cutting forces on the cutting edge appear in tangential (dFt) radial (dFr) and axial (dFa) forces acting on a differential flute element with height dz are expressed similar to Eqn 5.3:

$$\begin{aligned} dF_{t,j}(\phi,z) &= [K_{tc} h_j(\phi_j(z)) + K_{te}]dz \\ dF_{r,j}(\phi,z) &= [K_{rc} h_j(\phi_j(z)) + K_{re}]dz \\ dF_{a,j}(\phi,z) &= [K_{ac} h_j(\phi_j(z)) + K_{ae}]dz \end{aligned} \tag{5.3}$$

The instantenous chip thickness variation can be approxiamated as:

$$h_j(\phi,z) = c\sin\phi_j(z) \tag{5.4}$$

Where $\phi_j(z)$ is the immersion angle for the flute (j) at an axial depth of cut z and c is the feed per tooth.

The cutting constants can be evaluated from the mechanistic identification method or orthogonal cutting experiments. By accepting the helix angle (β) as the oblique angle of the end mill, the elemental forces are resolved into feed (x) normal (y) and (z) directions using the transformation:

$$\begin{aligned} dF_{x,j}(\phi_j(z)) &= -dF_{t,j}\cos\phi_j(z) - dF_{r,j}\sin\phi_j(z) \\ dF_{y,j}(\phi_j(z)) &= +dF_{t,j}\sin\phi_j(z) - dF_{r,j}\cos\phi_j(z) \\ dF_{z,j}(\phi_j(z)) &= +dF_{a,j} \end{aligned} \tag{5.5}$$

Adding the equation 5.3 and 5.4 into equation 5.5 leads to:

$$\begin{aligned} dF_{x,j}(\phi_j(z)) &= \left\{\frac{c}{2}\left[K_{tc}\sin 2\phi_j(z) - K_{rc}(1-\cos 2\phi_j(z))\right] + \left[K_{te}\cos\phi_j(z) - K_{re}\sin\phi_j(z)\right]\right\}dz \\ dF_{y,j}(\phi_j(z)) &= \left\{\frac{c}{2}\left[K_{tc}(1-\cos 2\phi_j(z)) - K_{rc}\sin 2\phi_j(z)\right] + \left[K_{te}\sin\phi_j(z) - K_{re}\cos\phi_j(z)\right]\right\}dz \\ dF_{z,j}(\phi_j(z)) &= \left[K_{ac}c\sin\phi_j(z) + K_{ae}\right]dz \end{aligned} \tag{5.6}$$

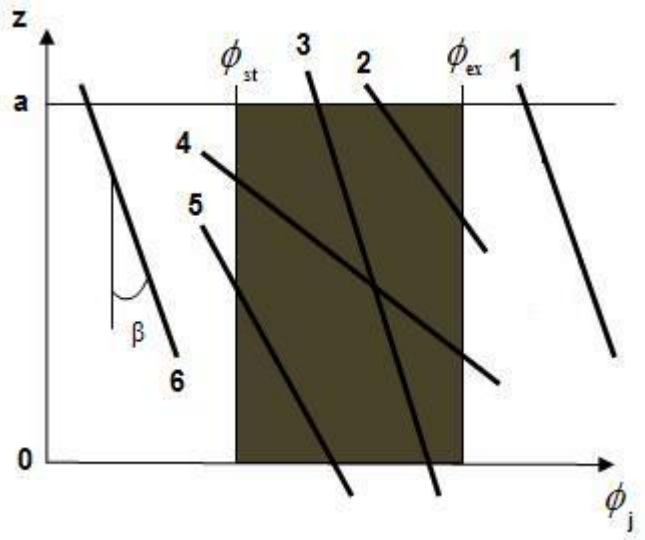

(a)

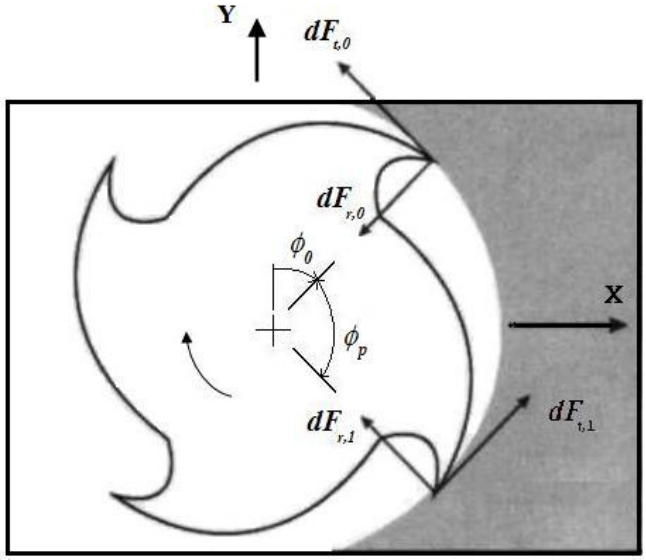

(b)

Figure 5.19: Helical Flute Part Face Integration Zones (a), and Differential Forces on The Cutting (b)

The total cutting force produced by the flute is calculated by the analytically integration of differential forces along the in cut portion of the flute j.

$$F_q(\phi_j(z)) = \int_{z_{j,1}}^{z_{j,2}} dF_q(\phi_j(z))dz \qquad q = x, y, z, \tag{5.7}$$

Where the lower and upper engagement limits of the in-cut portion of the flute j are $z_{j,1}(\phi_j\{z\})$ and $z_{j,2}(\phi_j\{z\})$ respectively. Integrations are carried out by noting $\phi_j(z) = \phi + j\phi_p - k_\beta z$ and $d\phi_j(z) = k_\beta dz$. Thus :

$$F_{x,j}(\phi_j(z)) = \left\{ \frac{c}{4k_\beta} \left[K_{tc} \cos 2\phi_j(z) + K_{rc} \left[\phi_j(z) - \sin 2\phi_j(z) \right] \right] + \frac{1}{k_\beta} \left[K_{te} \sin \phi_j(z) - K_{re} \cos \phi_j(z) \right] \right\}_{z_{j,1}(\phi_j(z))}^{z_{j,2}(\phi_j(z))}$$

$$F_{x,j}(\phi_j(z)) = \left\{ \frac{-c}{4k_\beta} \left[K_{tc} (2\phi_j(z) - \sin 2\phi_j(z)) + K_{rc} \cos 2\phi_j(z) \right] + \frac{1}{k_\beta} \left[K_{te} \cos \phi_j(z) + K_{re} \sin \phi_j(z) \right] \right\}_{z_{j,1}(\phi_j(z))}^{z_{j,2}(\phi_j(z))}$$

$$F_{z,j}(\phi_j(z)) = \frac{1}{k_\beta} \left[K_{ac} c \cos \phi_j(z) - K_{ae} \phi_j(z) \right]_{z_{j,1}(\phi_j(z))}^{z_{j,2}(\phi_j(z))}$$

(5.8)

The determination of axial integration limits $z_{j,1}$ and $z_{j,2}$ are necessary for each flute to implement the cutting force model. In Figure 5.18 possible helical flute–cutting zone intersections are shown. There are six distinct ways that a helical tooth j can interact. Therefore to determine the axial integration limits, the following agorithm in the Table 5.4 was developed was developed for six distinct cases.

Table 5.4: Integration Limits

Case	If	In\Out	$z_{j,1}$	$z_{j,2}$
1	$\phi_j(z=0) > \phi_{ex}$ & $\phi_j(z=a) > \phi_{ex}$	Out	-	-
2	$\phi_j(z=0) > \phi_{ex}$ & $\phi_j(z=a) < \phi_{ex}$ & $\phi_j(z=a) > \phi_{st}$	In	$(1/k_\beta)(\phi + j\phi_p - \phi_{ex})$	a
3	$\phi_{st} < \phi_j(z=0) < \phi_{ex}$ & $\phi_{st} < \phi_j(z=a) < \phi_{ex}$	In	0	a
4	$\phi_j(z=0) > \phi_{ex}$ & $\phi_j(z=a) < \phi_{ex}$ & $\phi_j(z=a) < \phi_{st}$	In	$(1/k_\beta)(\phi + j\phi_p - \phi_{ex})$	$(1/k_\beta)(\phi + j\phi_p - \phi_{st})$
5	$\phi_{st} < \phi_j(z=0) < \phi_{ex}$ & $\phi_j(z=a) < \phi_{st}$	In	0	$(1/k_\beta)(\phi + j\phi_p - \phi_{st})$
6	$\phi_j(z=0) < \phi_{st}$ & $\phi_j(z=a) < \phi_{st}$	Out	-	-

The values taken from the table above are substituted into Eqn. 5.8 and the total force per flute j is calculated. But to calculate the cutting forces contributed by each flute, case study in the table is repeated for all flutes and forces are summed to obtain the total instantenous forces on the cutter at immersion ϕ.

$$F_x(\phi) = \sum_{j=0}^{N-1} F_{xj} \;; \qquad F_y(\phi) = \sum_{j=0}^{N-1} F_{yj} \;; \quad F_z(\phi) = \sum_{j=0}^{N-1} F_{zj} \;; \tag{5.9}$$

The resultant cutting force acting on the milling cutter is:

$$F(\phi) = \sqrt{F_x(\phi)^2 + F_y(\phi)^2 + F_z(\phi)^2} \tag{5.10}$$

5.3.3 Mechanistic Identification of Cutting Constants in Milling

Orthogonal cutting parameters and mechanistic method are the two dinstict ways to determine the cutting constants in milling. It is possible to determine oblique cutting constants for a variety of milling cutter geometries by using orthogonal method. But this method is a non-practical method for complex cutter geometry and also evaluation of orthogonal data is a time consuming process. Since the mechanistic approach includes the effects of cutter and cutter edge geometry. It is more practical according to orthogonal approach. However, calculated cutting coefficients are special to that particular tool geometry and can be used with that tool only so the procedure must be repeated for each cutter geometry. Therefore mechanistic approach is limited but a quick method.

In mechanistic approach, a set of milling experiments are conducted at different feed rates with constant immersion and axial depth of cut. The aim of the experiments is to measure the average forces per tooth period. The measured average forces are equated to the analytically derived milling force expressions to calculate the cutting coefficients. $\varnothing_j = (z)$, $dz = a$, and $k_\beta = 0$ are replaced in Eqn. 5.6 and it is integrated over one revolution and divided by the pitch angle ($\varnothing_p = 2\pi / N$) and average milling forces per tooth period are evaluated.

$$\overline{F}_q = \frac{1}{\phi_p} \int_{\phi_{st}}^{\phi_{ex}} F_q(\phi) d\phi \tag{5.11}$$

Since the flute cuts only within the immersion zone (i.e., $\varnothing_{st} \leq \varnothing \leq \varnothing_{ex}$), integration of the instantaneous cutting forces leads to:

$$\overline{F_x} = \left\{ \frac{Nac}{8\pi}[K_{tc}\cos 2\phi - K_{rc}[2\phi - \sin 2\phi]] + \frac{Na}{2\pi}\left[-K_{te}\sin\phi + K_{re}\cos\phi \right] \right\}_{\phi_{st}}^{\phi_{ex}}$$

$$\overline{F_y} = \left\{ \frac{Nac}{8\pi}[K_{tc}[2\phi - \sin 2\phi] - K_{rc}\cos 2\phi] - \frac{Na}{2\pi}\left[-K_{te}\cos\phi + K_{re}\sin\phi \right] \right\}_{\phi_{st}}^{\phi_{ex}})()$$

$$\overline{F_z} = \frac{Na}{2\pi}\left[-K_{ac}c\cos\phi + K_{ae}\phi \right]_{\phi_{st}}^{\phi_{ex}}$$

(5.12)

In slot milling (full immersion), the entry and exit angles are $ø_{st} = 0$ $ø_{ex} = \pi$ respectively, therefore slotting is the most appropriate milling method account of the simplification of the process. If we apply the full immersion (slotting) conditions to equation (5.12); the avearge forces per tooth period are simplified as:

$$\overline{F_x} = -\frac{Na}{4}K_{rc}c - \frac{Na}{\pi}K_{re}$$

$$\overline{F_y} = +\frac{Na}{4}K_{tc}c + \frac{Na}{\pi}K_{te} \qquad (5.13)$$

$$\overline{F_z} = +\frac{Na}{\pi}K_{ac}c + \frac{Na}{2}K_{ae}$$

The average cutting forces are expressed by a linear function of feed rate (c) on offset contributed by the edge forces:

$$\overline{F_q} = \overline{F}_{qc}c + \overline{F}_{qe} \quad (q = x, y, z) \qquad (5.14)$$

The cutting edge components of equation (5.14), (F_{qc}, F_{qe}) are estimated by linear regression of the measured average forces at each feed rate. Finally evaluation of cutting force coefficients from equation (5.13) and (5.14) leads to:

$$K_{tc} = \frac{4\overline{F}_{yc}}{Na}, \quad K_{te} = \frac{\pi\overline{F}_{ye}}{Na},$$

$$K_{rc} = \frac{-4\overline{F}_{xc}}{Na}, \quad K_{re} = \frac{-\pi\overline{F}_{xe}}{Na}, \qquad (5.15)$$

$$K_{ac} = \frac{\pi\overline{F}_{zc}}{Na}, \quad K_{ae} = \frac{2\overline{F}_{zc}}{Na},$$

5.3.4 Cutting Constant Identification and Milling Force Simulation

To calculate the cutting constants (Krc, Ktc,Kac,Kre,Kte,Kae) of BMG-WC work-tool material pair, four set of slot milling cutting experiments, and to validate the results, six sets of slot milling cutting experiments were carried out at different feed rates. During the processes, cutting forces in three directions (x, y, z) were recorded and cutting constants of BMG-WC pair were calculated by using the mechanistic identification method in section 5.3.3. The spindle speed, feed rates and average of the experimentally measured forces in three directions of the milling experiments are shown in the Table 5.5.

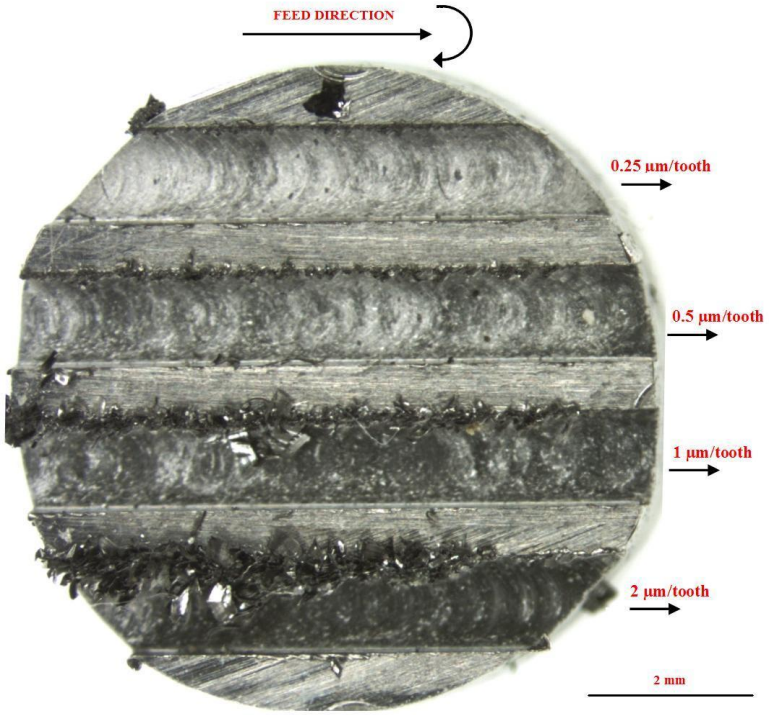

Figure 5.20: Slots Machined by 1 mm Diameter WC tool at Different Feed Rates.

It is clearly seen from the Figure 5.20 that surface roughness of the slots increases with the increasing feed rate at constant cutting speed.

Table 5.5: Slot Milling Experiments at 0.26 m\s Cutting Speed

EXP.	Feed Rate	Spindle Speed	Average of Cutting Forces (N)		
#	(µm/tooth)	(rpm)	Fx	Fy	Fz
			Feed	Normal	Axial
1	0.25	5000	3.81	2.32	0.15
2	0.5	5000	4.57	2.59	0.35
3	1	5000	5.7	3.28	0.04
4	2	5000	7.23	4.28	0.52

After application of the mechanistic identification method, the cutting coefficients in Table 5.6 were derivated from the linear regression of the data shown in Figure 5.21.

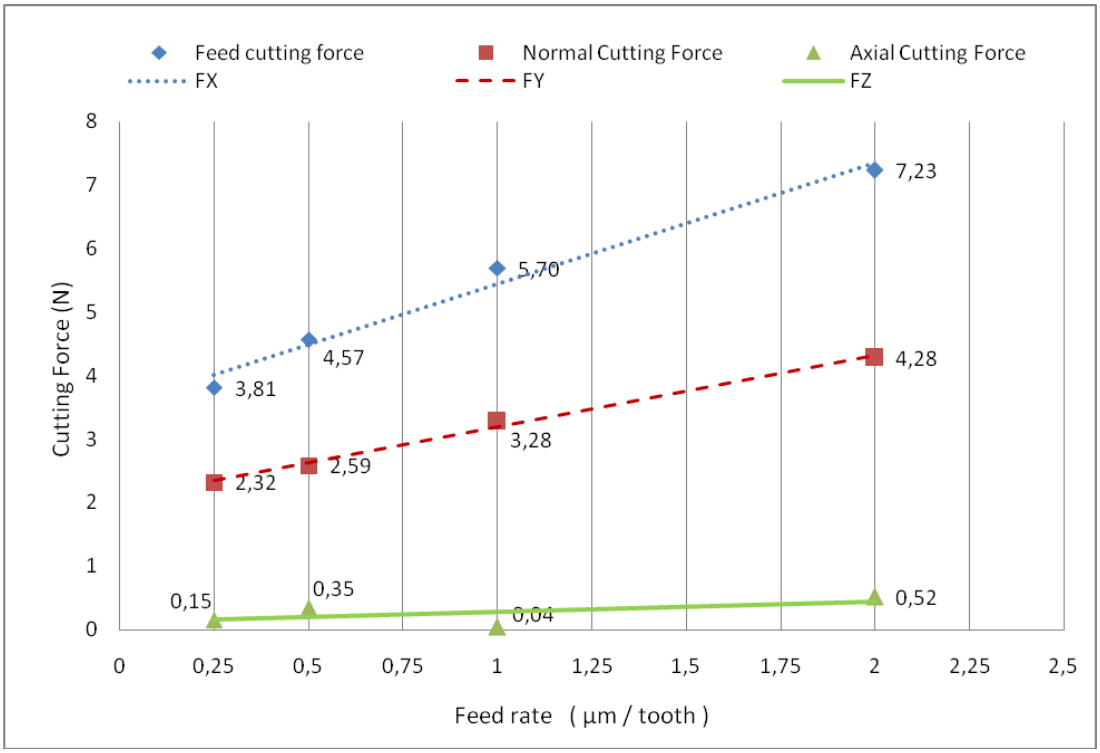

Figure 5.21: Cutting Force vs c (µm/tooth)

Table 5.6: Cutting Coefficients of Zr-Based BMG-WC Pair In The Range of 0.25-2 µm/tooth Feed Rate

K	Cutting ($N\backslash mm^2$)	Edge (N\mm)
Kr (radial)	7611.3	11.1349
Kt (tangential)	4513.8	6.4696
Ka (axial)	515.5	0.2263

The cutting coefficients above were inserted the milling force simulation algorithm in Matlab and analytical modeling of end milling forces for BMG-WC pair were constituted for a specified feed range. In the Figures 5.22, 5.23, and 5.24, the simulation of the cutting force period of validation experiments (2, 4, and 6) concave

the periodic data acquired by the dynonometer with less than 5% error rate. The results of the other validation experiments in Table 5.7 are close to the real values but the data acquired by the dynonometer is partially true because of the malfunction in the control unit.

Table 5.7: Validation Experiments

EXP. #	Feed Rate (μm/tooth)	Spindle Speed (rpm)
1	0.3	5000
2	0.75	5000
3	1.2	5000
4	1.5	5000
5	1.8	5000
6	3	5000

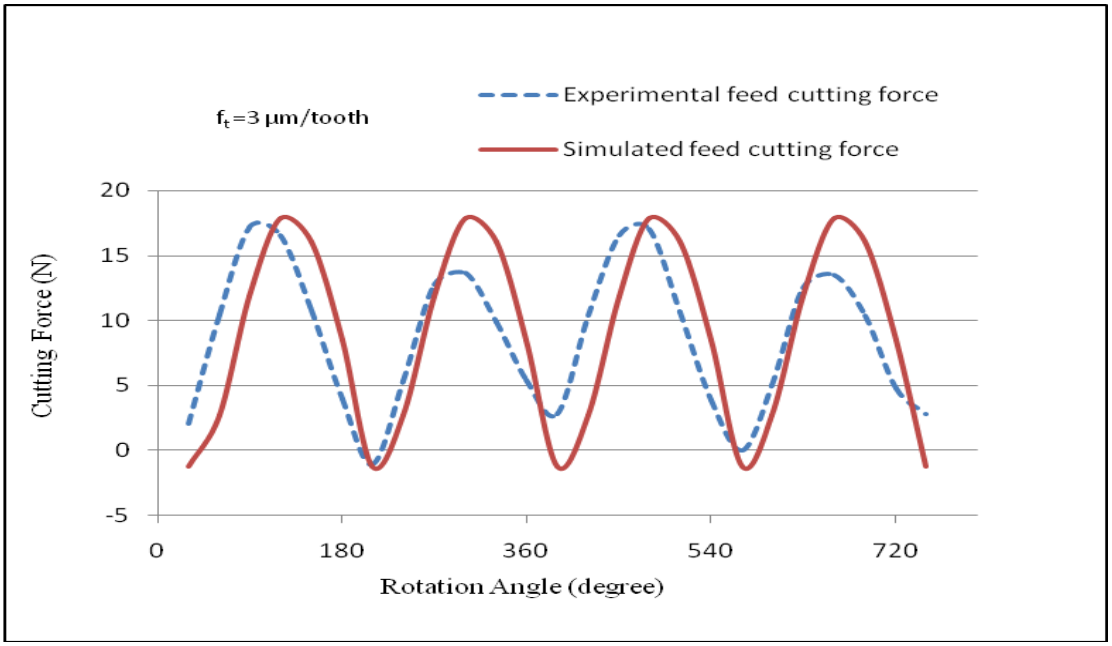

(a)

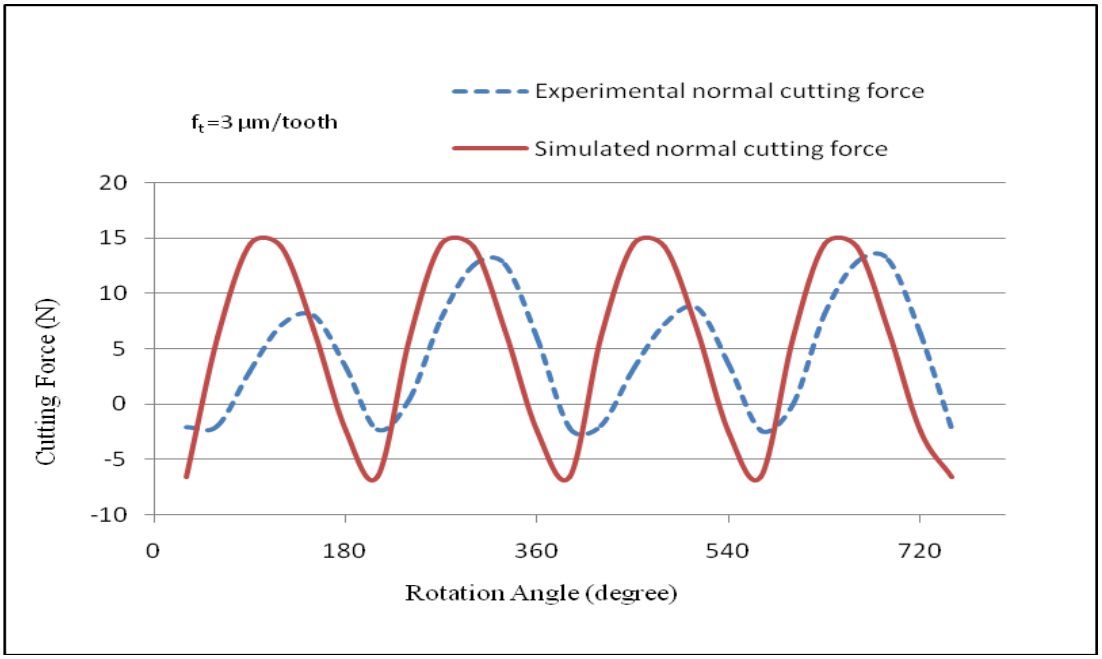

(b)

Figure 5.22: Comparison of Milling Force Simulation With Experimentally Recorded Force Along Feed Direction (a) and (b) Normal Direcion at 3 µm/tooth Feed Rate

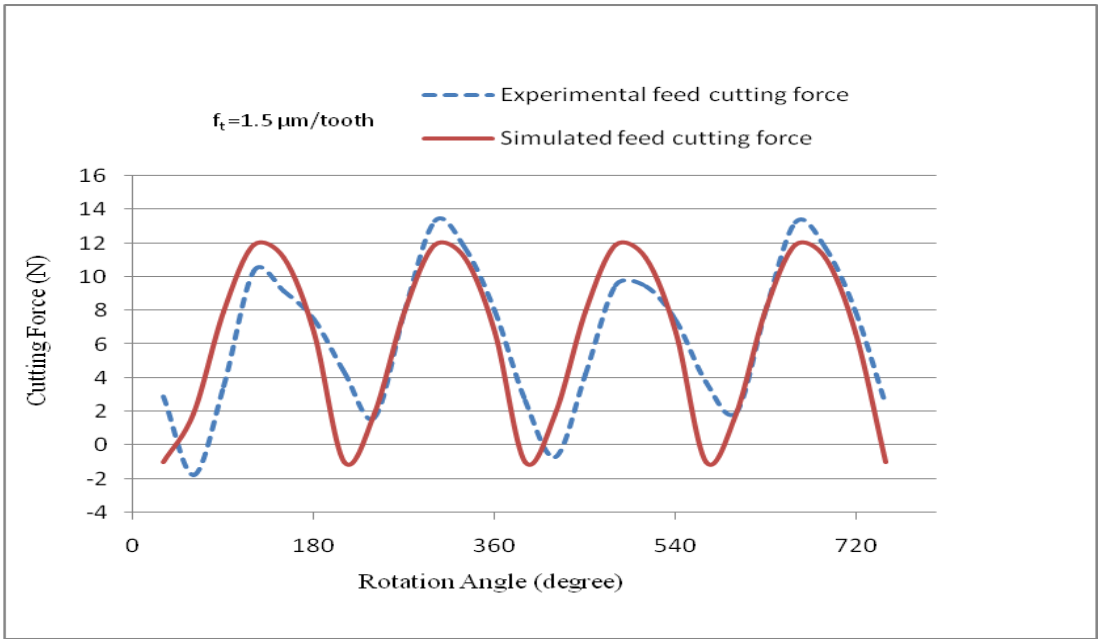

(a)

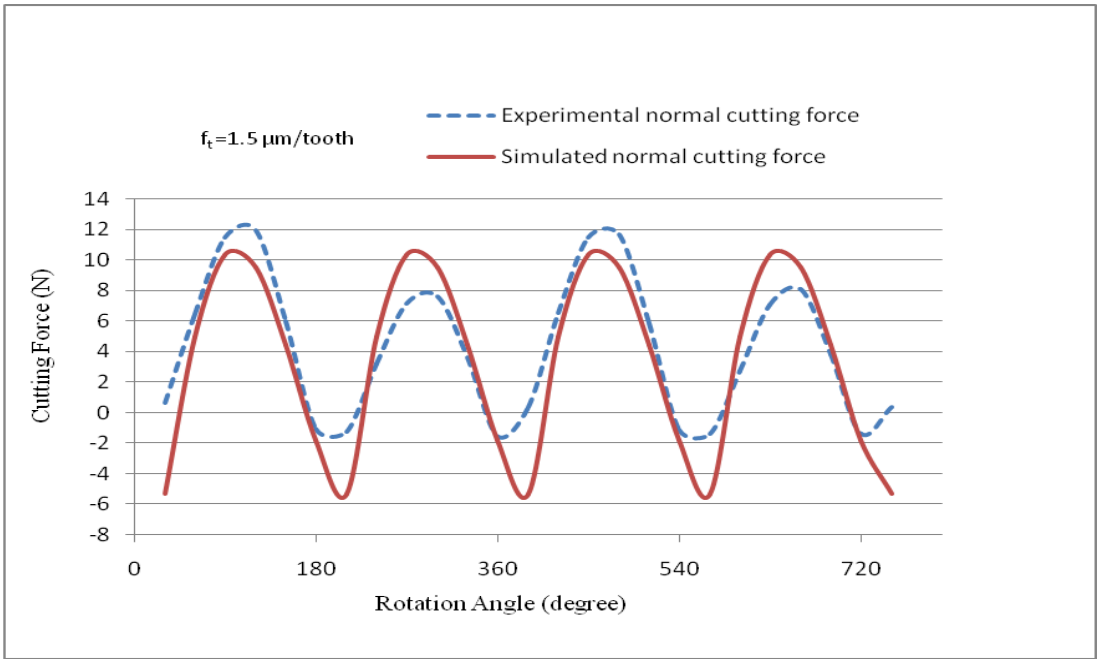

(b)

Figure 5.23: Comparison of Milling Force Simulation With Experimental Force for Feed (a) and (b) Normal Direcions at 1.5 µm/tooth Feed Rate and at 5000 rpm

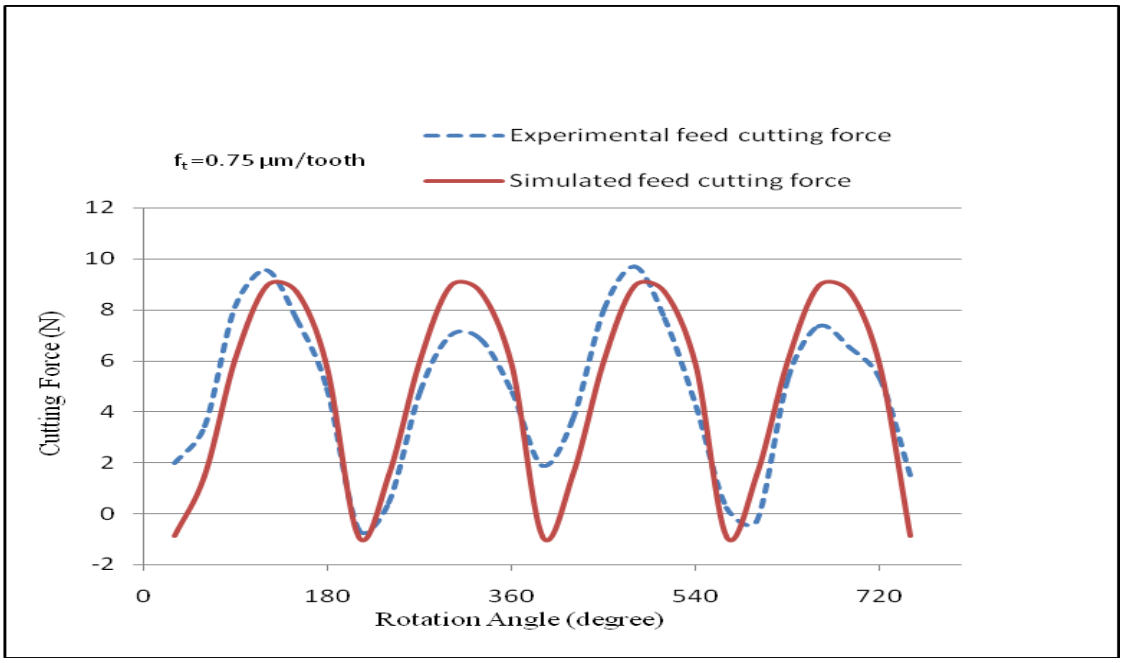

(a)

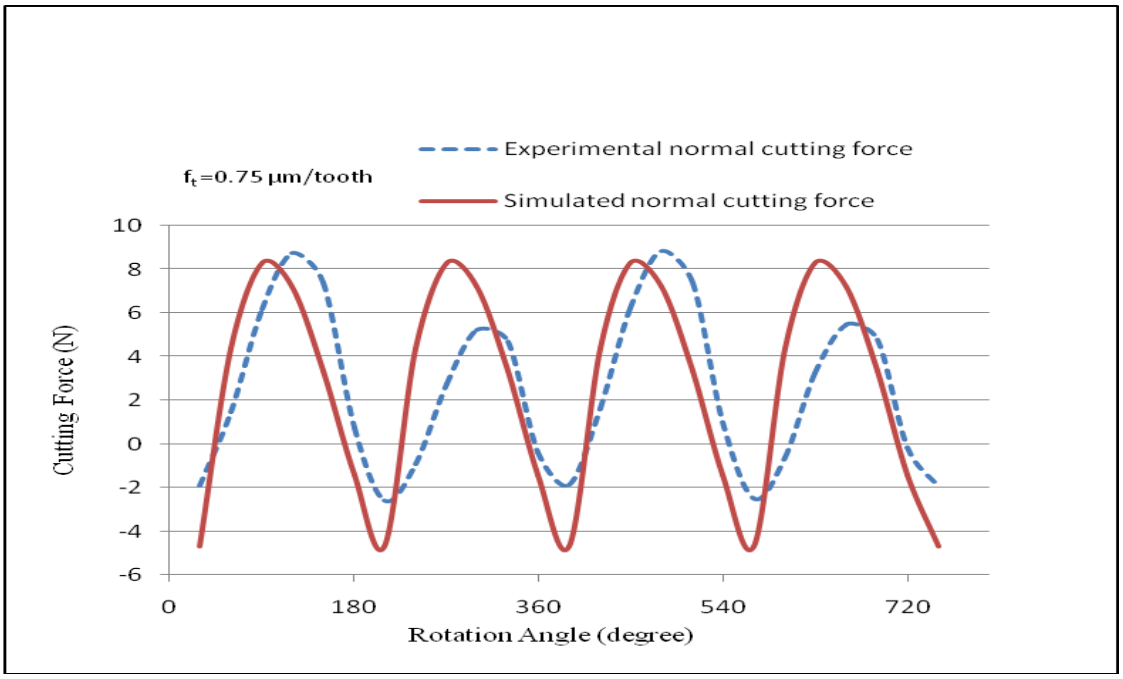

(b)

Figure 5.24: Comparison of Milling Force Simulation With Experimental Force for Feed (a) and (b) Normal Direcions at 0.75 µm/tooth Feed Rate and at 5000 rpm

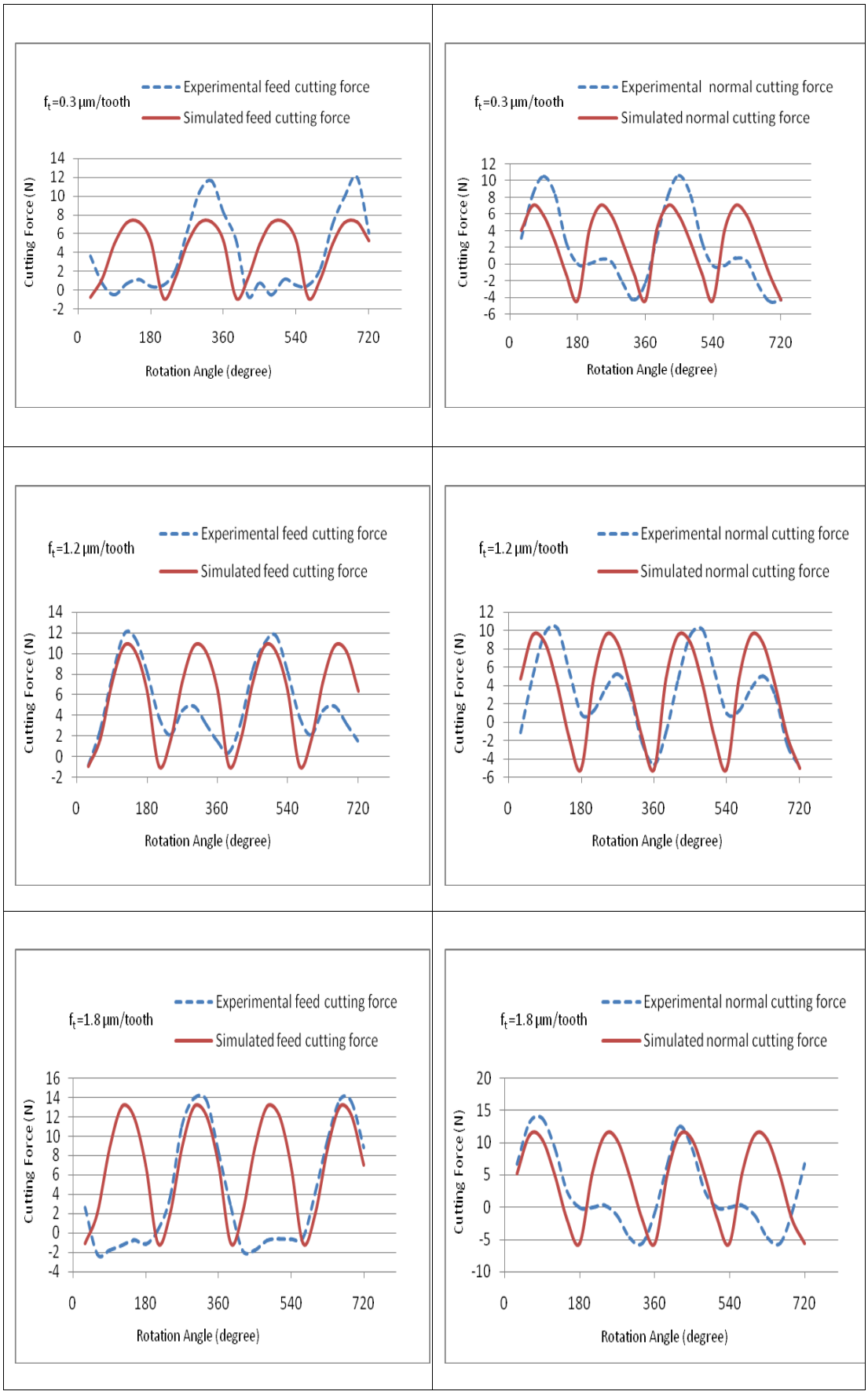

Figure 5.25: Experimental and Simulated Force Periods for Two Revolution.

5.3.5 Chip Morphology

Chip morphology in milling also varies in size and shape according to process parameters, work and tool materials and tool geometry. The tools traveled a spiral path (Figure 5.26) to use the limited workpiece efficiently during cuttings and for each cutting an unused new tool was used. Classification of chips according to ISO-based chip-form classification during spiral path cutting at different feed rates demonstrate that needle like and ribbon type chip morphology of BMG is observed in this feed range. These ribbon and needle like chips at three different feed rates are shown in Figure 5.27.

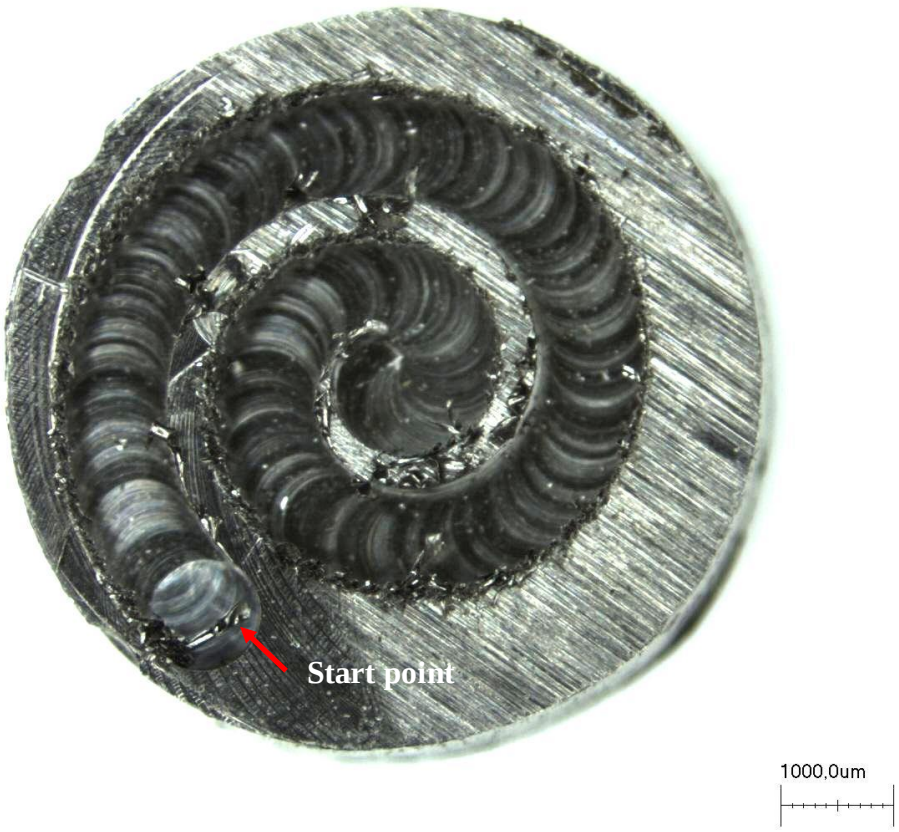

Figure 5.26: Machined BMG With Spiral Tool Path

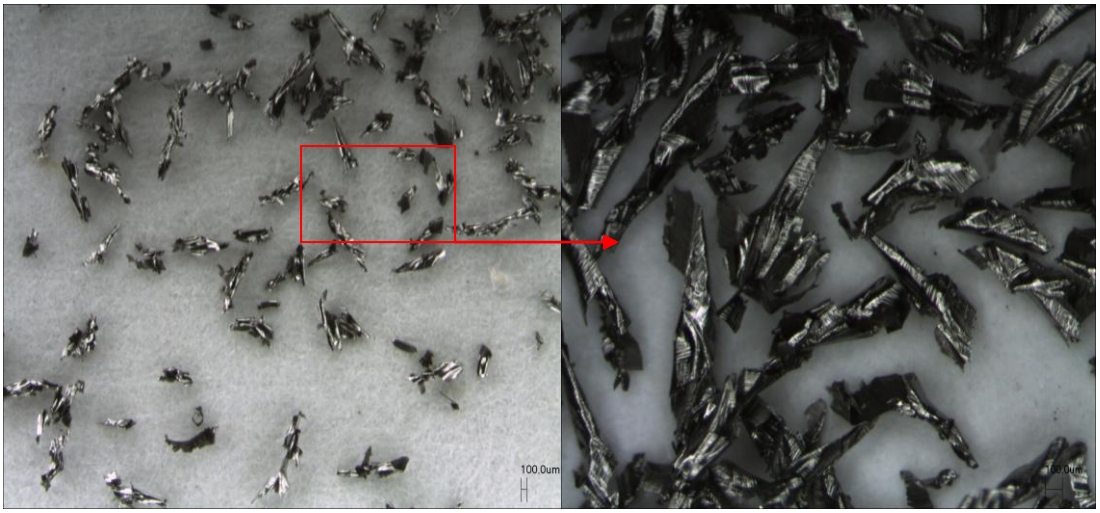

(a) Needle Like Chips Form at 0.5 µm/tooth With 0.5 mm Depth of Cut

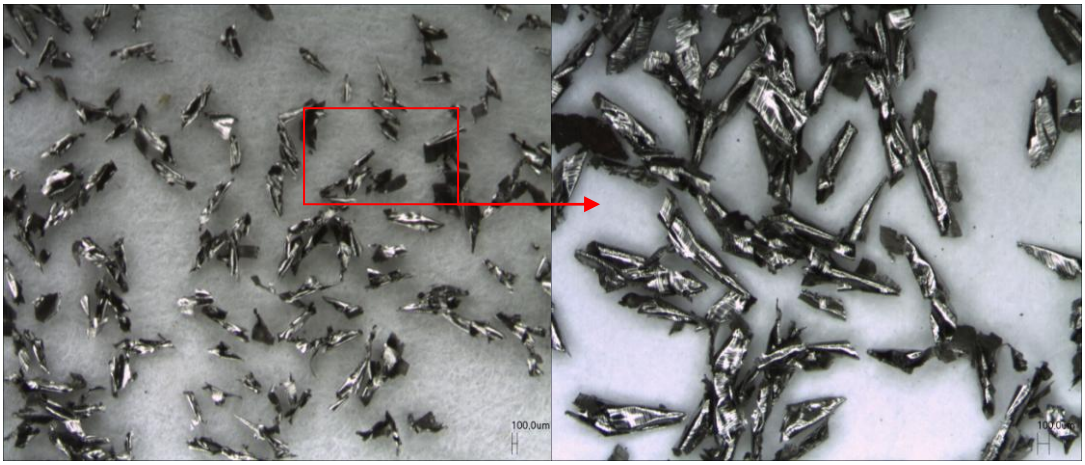

(b) Needle Like Chips Form at 1 µm/tooth With 0.5 mm Depth of Cut

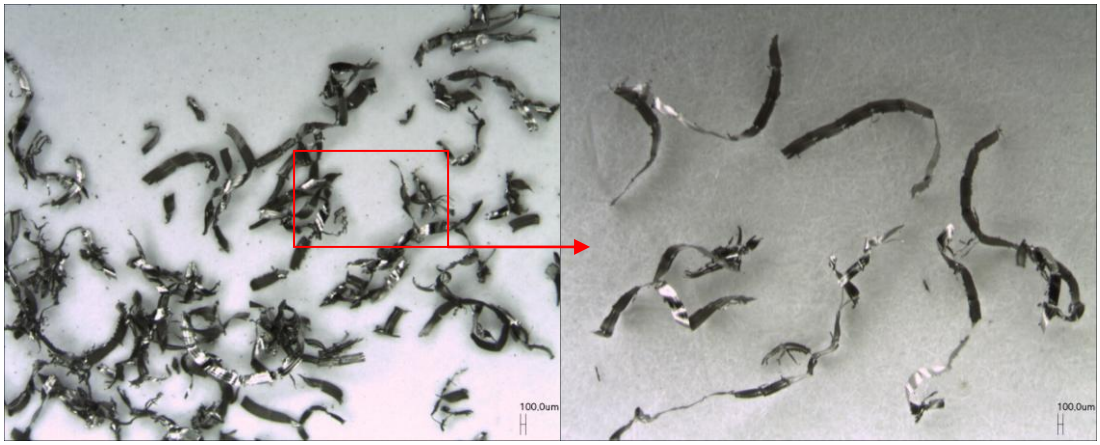

(c) Ribbon Type Chips Form at 2 µm/tooth With 0.5 mm Depth of Cut

Figure 5.27: Chip Morphology of Spiral Milled BMG at 0.5 µm/tooth (a) 1 µm/tooth (b) 2 µm/tooth (c)

5.3.6 Burr Formation

Burr formation is similar to chip formation and occurs at the end of the cutting. It is hazardous in handling machined parts and can intercede with the assembly of parts. In this study, burrs formed in slot milled BMG workpiece are examined and top burr and rollover type burr are observed. The rollover type burr is a partially formed chip which is also known as an exit burr. This type of burr is formed by bending in the direction of the cutting velocity at the end of a cut in face-milling. The poisson burr which result from the workpiece material's tendency to bulge in the direction parallel to the cutting edge when compressed by flank forces on the tool [68]. The top burr is the combination of tear and poisson burr is observed along the one side of the slot in Figure 5.28. Since the size of top burr is substantially smaller than exit type of burr, deburring operation for top burr is not necessary for conventional cutting processes. However, the radius of the cutting edge is larger compared to the feed per tooth so that top burrs are comperatively larger in micro milling operations. Also, partially formed chips are deposited along the other side of the slot because of the relative velocity between the feed and spindle speed. Increasing the feed rate at constant spindle speed increase the amount of deposition along one side of the slot but increasing cutting speed at constant feed causes decrease in deposition. This results from the effect of the relative velocity on the chip transferring. It is obviously seen from the Figure 5.29 that the amount of burr formed from the deposited chips increase with the increase in feed rate while the cutting speed is constant. When considering the burr formation mechanisms, the main reason of burr formation while machining of the BMG is the large elastic strain of it. Burrs are also associated with tool wear. However, since an unused new tool was used for each cutting operation, there is no tool wear effect on burr formation in our study [71-73].

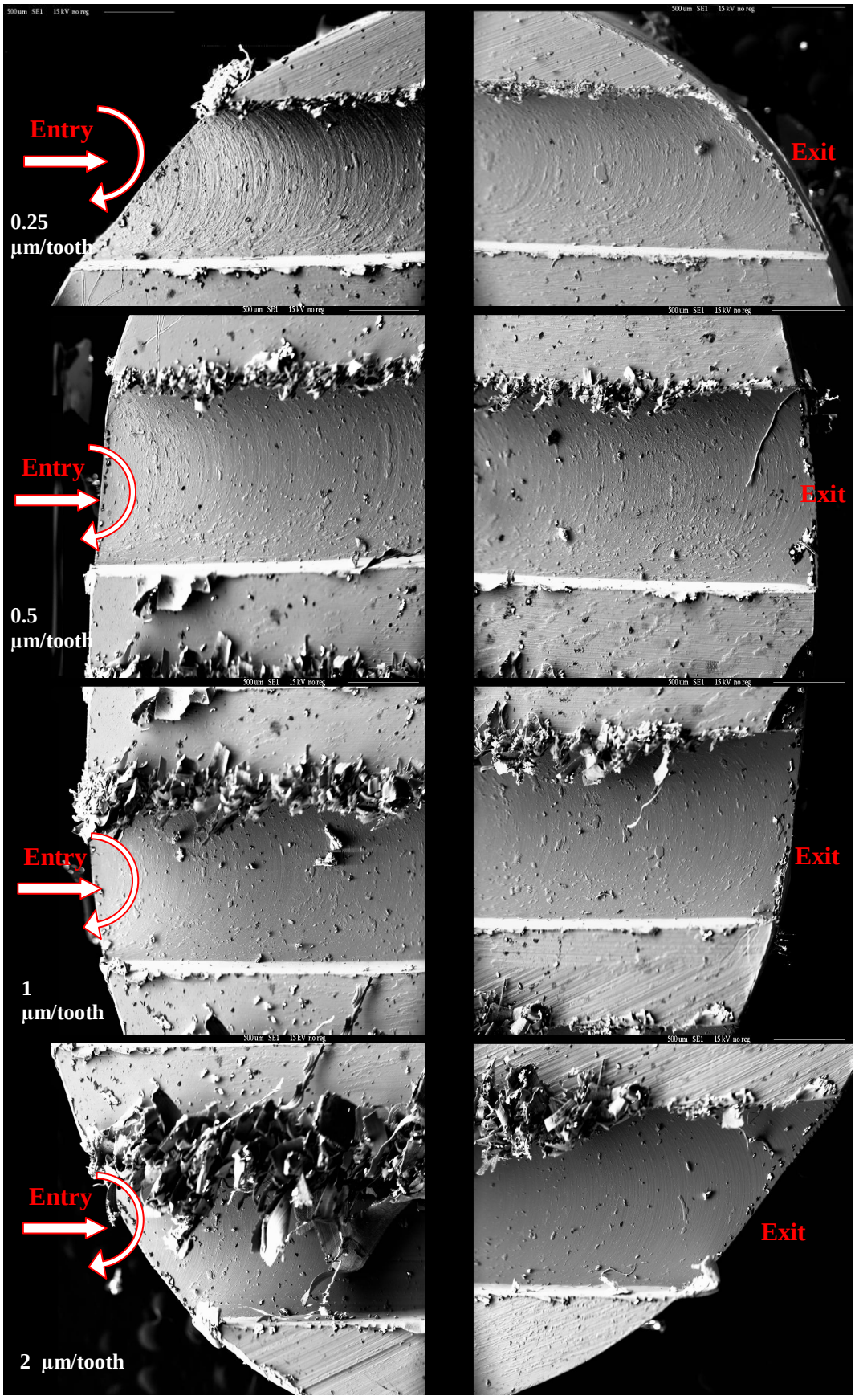

Figure 5.28: Burr Formations in Slot Milling of Zr-based BMG

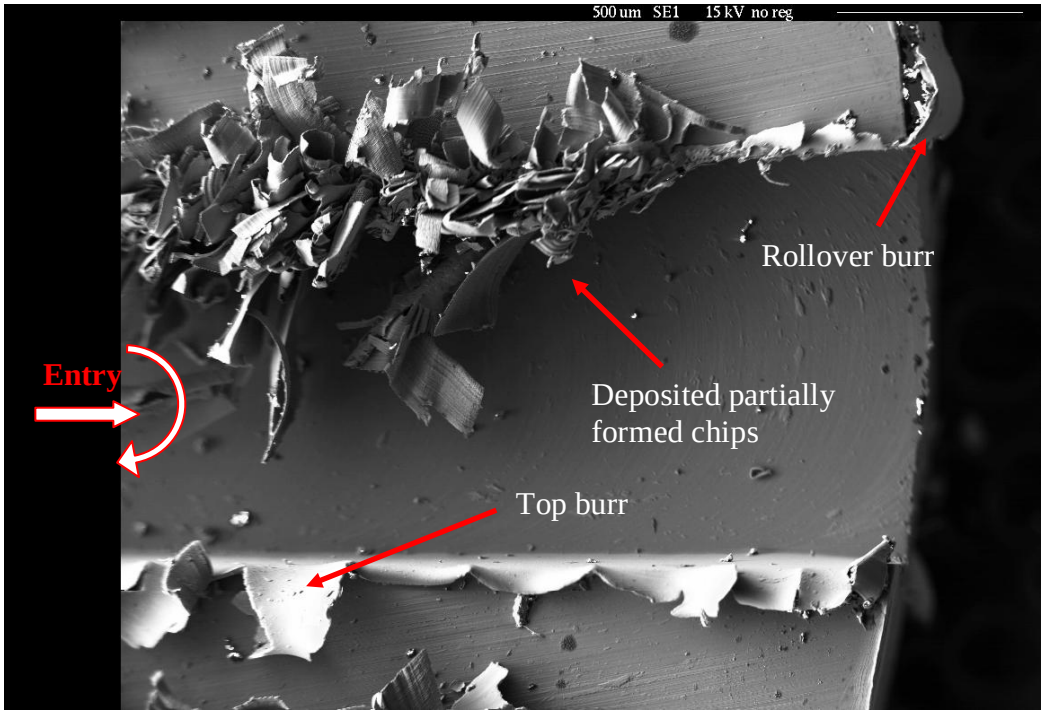

Figure 5.29: Detailed Views of Burrs on Zr-based BMG

5.3.7 Surface Roughness

The measurement of surface roughness is among important aspects of manufacturing. Surface of a material affect the materials corrosion, fatigue, wear, friction, thermal and electrical conductivity. In this study surface roughness of the slots as shown in Table 6 were measured by using a profilometer. Results present that low feed rates provides better surface roughness. Each result in the Table 5 was calculated by taking the average of three measure of profilometer. Resultant surface roughness values for milling are in the range of grinding process roughness range. This result shows that it is easy to get good surface finish in BMG parts even with conventional machining processes. Best surface quality was obtained at lowest feed rate.

Table 5.8: Surface Roughnesses of Milled Slots

Feed Rate (µm/tooth)	R_a (µm)	R_z (µm)	R_{max} (µm)
0.25	0.115	0.68	1.17
0.5	0.344	2.413	3.224
1	0.576	3.09	4.76
2	0.801	3.63	4.73

6. RESULTS & DISCUSSION

In this research, effects of tool material and feed rate for BMG drilling were studied. Two different tool material MG-WC and solid-WC were used in drilling operations. Thrust force measurement test results showed that MG-WC tool creates almost 15 % more thrust force than one TiAlN coated WC tool. Higher feed rates create higher thrust force for BMG drilling. Making a double increase on the feed rate, the thrust force becomes about 20 percent higher. Chip morphology, burr formation and hole surface in drilling of BMG was also investigated. No chip light emission was observed because of the low spindle speed so not to cause light emission slow feed rates for BMG is recommended at lower than 2500 rpm spindle speeds for WC tools. There is no entrance burr formation observed. Crown shape burr formation is identified on most of the hole exits. MG-WC tool used hole shows no exit burr formation at 5 mm/min (1 μm/rev) feed rate. Two traditional types of BMG chip morphology ribbon shape snarled chips and helical shape snarled chips were observed. Because of the low thermal conductivity of the BMG, heat formed during drilling can not remove quickly so excess heat cause BMG to be soften and more ductile. This event is the reason for the wrapping of chip around the tools. The tools with chip-breaking grooves in flute can be used to prevent the wrapping of chip around the tool. Hole surface roughness measurement results also confirmed that MG-WC tool shows better drilling performance on BMG drilling at given conditions.

In this study, slot milling was conducted to investigate the mechanics of milling processes of Zr-based BMG and milling with spiral tool path was conducted to examine chip morphology, burr formation and thermal analysis of BMG. The reason to follow the spiral tool path is to use the limited BMG efficiently. Cutting mechanics of helical end mill was investigated and for a specified feed range the cutting coefficients of BMG were calculated and cutting force model was created. The analytically modeled forces verify the experimental values with less than 5% error. The rollover type burr is observed at exit of the slot and the top burr is observed along the slot. Beside that ribbon and needle like chips are observed in spiral milling. Among them needle like chip is more preferable because of the machinability and it is observed at lower feed rates. Also results showed that the

increasing feed rate at constant spindle speed causes increase in the amount of deposited chip.

As a result, no chip light emission was observed during all cutting operations and temperatures weren't reached the crystallization temperatures also. The previous researches exhibited high cutting speed results light emission in drilling processes. Our study exhibited that low feed rate and higher cutting speed is better for surface roughness and chip morphology for milling of Zr-based BMG. However, the surface roughness of drilled holes decreases with the increasing feed rate. Therefore high feed rates and low cutting speeds are more suitable for drilling of BMG. In addition suitable tools should be selected to improve surface quality and tool life. Hundred percent glassy structure of BMG makes its machinability harder than most of the conventional metals. New developed partially nano crystallized BMG composites which have higher toughness and ductility can show better machinability.

REFERENCES

[1] **Peker, A. and Johnson W.L.**, 1993. A highly processable metallic glass, Zr41Ti14Cu12.5Ni10Be22.5, *Appl. Phys. Lett*, **63**, 2342-2344

[2] **F. Spaepen.**, 1975. On the fracture morphology of metallic glasses, *Acta. Metallurgica,* **23,** 615–620.

[3] **Bakkal, M., Liu, C.T., Watkins, T.R., Scattergood, R.O. and Shih**, **A.J.,** 2004. Oxidation and crystallization of Zr-based bulk metallic glass due to machining, *Intermetallics*, **12,** 195–204.

[4] **Bakkal, M., Shih, A.J., McSpadden, S.B. and Scattergood**, **R.O.** 2005. Thrust Force, torque, and tool wear in drilling of bulk metallic glass *International Journal of Machine Tools and Manufacture***, 45**,

[5] **Sneiderman P.**, 1998. "Metallic glass: material of the future?" *Headlines of Hopkins*, Johns Hopkins University News Release

[6] **Klement W., Willens R. H. and Duwez P**., 1960. "Non-crystalline structure in solidified gold-silicon alloys," *Nature,* **187**, pp. 869-870.

[7**]** **Duwez, P., Willens R. H. and Klement W**., 1960. "Continuous series of metastable solid solutions in silver-copper alloys," *Journal of Applied Physics*, **31**, 1136-1137.

[8] **Chen, H.S. and D., Turnbull,** 1968. "Evidence of a glass-liquid transition in a Au-Ge-Si Alloy," *Journal of Chemical Physics*, **48**, 2560-2571.

[9] **Johnson, W.L**., 1999. "Bulk Glass-Forming Metallic Alloys: Science and Technology," *Materials Research Bulletin*, **24/10**, 42-56.

[10] **Kasvesh, S**., 1978. Metallic Glasses, *ASM International*, Metals Park, Ohio,

[11] **Chen, H.S**., 1974. "Thermodynamic consideration of formation and stability of metallic glass," *Acta Metallurgica*, **22**, 1505-1511.

[12] **Chen, H.S**., 1976. "Glass temperature formation and stability of Fe, Co, No, Pb and Pt based glasses," *Materials Science and Engineering*, **23**, 151-154.

[13] **Inoue, A., Yamaguchi, H. and Zhang, T.,** 1990. "Al-La-Cu Amorphous Alloys with a wide supercooled region," *Materials Transaction, The Japan Institute of Metals*, **31**, 104-109.

[14] **Inoue, A., Nakamura, T., Nishiyama, N. and Masumoto, T**., 1992. "Mg-Cu-Y Bulk Amorphous-Alloys with a wide supercooled region," *Materials Transaction, The Japan Institute of Metals*, **33**, 937-945.

[15] **Inoue, A., Zhang, T. and Nishiyama, N.,** 1993. "Preparation of 16mm diameter rod of amorphous Zr65Al7.5Ni10Cu17.5 Alloy," *Materials Transaction, The Japan Institute of Metals*, **34**, 1234-1237.

[16] **Peker, A. and Johnson, W. L.**, 1993. "A highly processable metallic glass Zr41.5Ti13.8Cu12.5Ni10Be22.5," *Applied Physics Letters*., **63**, pp. 2342-2344.

[17] **Inoue A., Nishiyama N. and Matsuda Y.,** 1996. "Preparation of bulk glassy Pd40Ni10Cu30P20 alloy of 40 mm in diameter by water quenching," *Materials Transactions, The Japan Institute of Metals*, **37/2**,181-184.

[18] **Lu Z. P.,** 2000. Glass Forming Ability and lass Transition study of rare-Earth Based Bulk Metallic Glasses, *PhD Thesis*, National University of Singapore.

[19] **Beck, H., Guntherodt, H-J.,** 1981. Glassy Metals I, *Topics in Applied Physics*, **46/1981,** 1-18

[20] **Klement, Willens and Duwez**, 1960. "*Non-Crystalline structure in solidified Au- Si alloys*" , Nature 187, 869

[21] **Anantharaman, T.R**., 1984. Metallic Glasses: Production, Properties and Applications, Trans Tech SA, Switzerland

[22] http://www.liquidmetal.com

[23] **Inonue,** 1998. Bulk Amorphous Alloys, Preparation and Fundamental Characteristics, Trans Tec Publications Ltd, Winterthur, Switzerland

[24] **Kalpakjian, S. and Schmid, S.R.,** 2003. Manufacturing Process for Engineering Materials, 4 th. Edition, Prentice Hall, New Jersey

[25] **Altintas**, **Y.,** 2000. Manufacturing Automation, Cambridge University Press, Cambridge

[26] **Laws, K.J., Gun, B. and Ferry, M.,** 2007. Materials Science and Engineering , **475**, 348-354

[27] **Ikarashi K.**, **Mizushima T., Makino A. and Inoue A.**, 2001. *Mater Sci Eng*, **304-306**, 763-766

[28] **Peker, A. and Johnson, W.L.**, 1993. *Appl. Phys. Lett.*, **63**, 2342.

[29] **Dougherty**, **G.M., Shiftlet, G.J. and Poon, S.J.,** 1994. *Acta Metall. Mater.*, **42**, 2275

[30] **Ozaki, K., Nishio, T., Matsumoto, A. and Kobayashi, K.,** 2004 *Mater. Sci. Eng.* A, **375**,857.

[31] **Tokita, M. J. and Powder Soc.,** 1995. *Technol., Jpn*. **30**, 790.

[32] **Choi, P.P., Kim, J.S., Nguyen, O.T.H. and Kwon, Y.S.,** 2007. *Materials Letters*, **61,**4591–4594

[33] **Ashby, M.F. and Greer, A.L.,** 2006. *Scripta Materialia*, **54**, 321–326.

[34] **Schroers, J. and Johnson, W.L.,** 2004. *Physical Review Letters*, **93,** 255 506.

[35] **Conner, R.D., Johnson, W.L., Paton, N.E. and Nix, W.D.,** 2003. *Journal of Applied Physics*, **94,** 904–911.

[36] **Schroers**, **J.,** 2005. *JOM – Journal of Metals*, **57**, 35– 39.

[37] **Schroers, J. and Paton, N.**, 2006. *Advanced Materials & Processes*,**164**, 61–63.

[38] **Leamy, H.J., Chen, H.S. and Wang, T.T.,** 1972. *Metallurgical Transactions*, **3**, 699.

[39] **Pampillo, C.A. and Chen, H.S.,** 1974. *Materials Science and Engineering*, **13**, 181–188.

[40] **Nishiyama, N. and Inoue, A.,** 1999. *Materials Transactions Jim*, **40**, 64–71.

[41] **Saotome, Y., Itoh, K., Zhang, T. and Inoue, A.,** 2001. *Scripta Materialia*, **44**, 1541–1545.

[42] **Schroers, J., Pham, Q. and Desai, A.,** 2007. *J. Mems*, **16,** 240.

[43] **Kawamura, Y., Kato, H., Inoue, A. and Masumoto, T.,** 1995. *Applied*

Physics Letters, **67,** 2008–2010.

[44] **Karaman, I., Robertson, J., Im, J.T., Mathaudhu, S.N., Luo, Z.P. and Hartwig, K.T.,** 2004. *Metallurgical and Materials Transactions A – Physical Metallurgy and Materials Science*, **35A**, 247–256.

[45] **Zhang, T., Tsai, A.P., Inoue, A. and Masumoto, T.,** 1992. *Science Reports of the Research Institutes Tohoku University Series A – Physics Chemistry and Metallurgy*, **36**, 261–271.

[46] **Schroers, J., Nguyen, T., and Croopnick, G.A.,** 2007. *Scripta Materialia,* **56,** 177–180.

[47] **Kundig, A.A., Schweizer, T., Schafler, E. and Loffler, J.F.** 2007. *Scripta Materialia*, **56**, 289–292.

[48] **Schroers, J., Pham, Q., Peker, A., Paton N. and Richard V. C.,** 2007. *Scripta Materialia*, **57**, 341–344

[49] **Lee K., Yun, E., Lee, S. and Kim**, **N. J.,** 2005. *Materials Science and Engineering A,* **408**, 92–101

[50] **Qiu'j, K., Yu, B. and Ren Y.,** 2007. *Journal of University of Science and Technology Beijing*, **14**, 59

[51] **Brothers JA.H. and D.C. Dunand.**, 2006. Amorphous metal foams, *Scripta Muter.,* **54**, 5 13.

[52] **Hufnagel, T.C., Fan, C., Ott, R.T. and Li, J.,** 2002. *Brennan Intermetallics* **10**, 1163–1166

[53] **Qin, C., Zhang, W., Amiya, K., Asami, K. and Inoue, A.,** 2007. *Materials Science and Engineering A*, 230–234

[54] **Qin, C.L., Zhang, W., Asami, K., Kimura, H., Wang, X.M. and Inoue, A.,** 2006. Acta Materialia, **54**, 3713–3719

[55] **Jiang, Q.K., Qin, C.L., Amiya, K., Nagata, S., Inoue, A. Zheng, R.T., Cheng, G.A., Nie, X.P. and Jiang J.Z.,** 2007. *Intermetallics*, 1-5

[56] **Inoue, A.,** 1998. Bulk Amorphous Alloys, *Tans Tech Publications*, Zurich,

[57] **Wang, W.H., Dong, C. And Shek C.H.,** 2004. *Materials Science and Engineering R,* **44** , 45–89

[58] **Li, Y., Ng, S.C., Lu, Z.P., Feng, Y.P. and Lu, K.,** 1998. *Phil. Mag. Lett.*, **78** 213

[59] **Xing, L.Q., Eckert, J., Lo¨ser, W., Roth, S., Schultz, L.,** 2000. *J. Appl. Phys.,* **88,** 3565.

[60] **Inoue, A., Zhang, T., Takeuchi, A. and Zhang, W.,** 1996. *Mater. Trans. JIM,* **37,** 636.

[61] **Wei, B.C., Wang, W.H., Pan, M.X. and Han, B.S.,** 2001. *Phys. Rev. B,* **64** , 012406

[62] **He, Y., Price, C.E. and Poon, S.J. Phil.,** 1994. *Mag. Lett.,* **70**, 371.

[63] **Ishihara, S., Zhang, W., and Inoue A.,** 2002. *Scripta Materialia,* **47** 231–235

[64] **Wang, W.H., Dong, C. and Shek C.H.,** 2004. *Materials Science and Engineering R,* **44,** 45–89

[65] **Li, H.X., Jung, H.Y. and Yi S.,** 2008. J*ournal of Magnetism and Magnetic Materials,* **320**, 241–245

[66] **Inoue, A. and Takeuchi, A.,** 2002. *Mater. Trans. JIM,* **43,** 1892.

[67] **Wang, W.H., Dong, C. and Shek C.H.,** 2004. *Materials Science and Engineering R,* **44**, 45–89

[68**]** **Stephenson, D. A. and Agapiou, J. S., 2007.** "Metal Cutting Theory and Practice", CRC Press, New York

[69] **Boothroyd**, **G.,** 1975. **"**Fundemantals of Machining and Machine Tools", McGraw-Hill, New York

[70] **Koenigsberger, F. and Tlusty, J.,** 1967. Machine Tool Structures, Vol.I: Stability Against Chatter, Pergamon Press,

[71] **Hashimura, M., Hassamontr, J. and Dornfeld D.A.,** 1999. Effect of in-plane exit angle and rake angles on burr height and thickness in face milling operation. *JManuf Sci Eng*, **121**, 13–9.

[72] **Lee K. and Dornfeld D.A.,** 2002. An experimental study on burr formation in micro-milling aluminum and copper, *Trans North Am Manuf Res Inst,* **30**, 255–62.

[73] **Lee, K. and Dornfeld, D.A.,** 2005. *Precision Engineering,* **29**, 246–252

[74] **Inoue, A., Shen, B.L. and Chang C.T.,** 2006. *Intermetallics,* **14,** 936–944

[75] **Inoue, A., Shen, B.L., Koshiba, H., Kato, H. and Yavari A.R.,** 2004. *Acta Materialia*, **52**, 1631–1637

[76] **Inoue, A. Shen, B.L. and Chang C.T.,** 2004. *Acta Materialia* **52**, 4093–4099

[77] **Inoue,A., Zhang, W., Tsurui, T., Yavari, A.R. and Greer, A.L.,** 2005. *Philos. Mag. Lett.*, **85,** 221–229.

[78] **Inoue, A., Shen, B.L. and Chang C.T.,** 2006. *Intermetallics,* **14**, 936–944

[79] **Qin, C.L., Zhang, W., Asami, K., Kimura, H., Wang, X.M. and Inoue, A.,** 2006. *Acta Materialia* **54**, 3713–3719

[80] **Jiang, Q.K., Zhang, G.Q., Yang, L., Wang, X.D., Saksl, K., Franz, H., Wunderlich, R., Fecht, H. and Jiang, J.Z.,** 2007. *Acta Materialia,* **55,** 4409–4418

[81] **Lee, K.A., Kim, Y.C., Kim, J.H., Lee, C.S., Namkung, J. and Kim M.C.,** 2007. *Materials Science and Engineering* A, **449–451**, 181–184

[82] **Chen, D., Takeuchi, A. and Inoue, A.,** 2007. *Materials Science and Engineering* A, **457**, 226–230

[83] **Chen, L.Y., Fu, Z.D., Zeng, W., Zhang, G.Q., Zeng, Y.W., Xu, G.L., Zhang, S.L. and Jiang, J.Z.,** 2007. *Journal of Alloys and Compounds*, **443**, 105–108

[84] **Xia, L., Shan, S.T., Ding, D. and Dong, Y.D.,** 2007, *Intermetallics*, **15**, 1046 -1049

[85] **Qin, C., Zhang, W., Amiya, K., Asami, K. and Inoue, A.,** 2007. *Materials Science and Engineering* A, **449–451** 230–234

[86] **Chen, L.Y., Hu, H.T., Zhang, G.Q. and Jiang J.Z.,** 2007. *Journal of Alloys and Compounds*, **443,** 109–113

[87] **Ding, C., Takeuchi, A. and Inoue, A.,** 2007. *Trans. Nonferrous Met. SOC China*, **17**, 1220-1224

[88] **Tian, W., Pang, S., Men, H., Ma, C. and Zhang, T.,** 2007. *Journal of University of Science and Technology*, **14**, 43

[89] **Zhang, Q.S., Zhang, W., Xie, G.Q., Nakayama, K.S., Kimura, H. and**

Inoue, A., 2007. *Journal of Alloys and Compounds*, **431**, 236–240

[90] **Li, H.X., Jung, H.Y. and Yi, S.,** 2008. *Journal of Magnetism and Magnetic Materials*, **320,** 241–245

CURRICULUM VITAE

Veli Nakşiler was born on March 12, 1982 in İstanbul, Turkey as the only son of Nazire and Neşad Nakşiler and brother of Nurdan and Zeynep Nakşiler. He graduated from Rıfat Canayakın High School in 2000 and started to Mechanical Engineering Department of İzmir Institute of Technology, in İzmir, in the same year. He turned back to İstanbul in 2005 after graduated from İzmir Institute of Technology as Mechanical Engineer. In the same year, he was admitted to Material and Manufacturing master program of Faculty of Mechanical Engineering in İstanbul Technical University. On November 28, 2005, he became a research assistant at the same department and still he works there. He is interested in football, snooker, drum and poem.